











RESEARCH ARTICLE

ATP Synthase K⁺- and H⁺-Fluxes Drive ATP Synthesis and Enable Mitochondrial K⁺-“Uniporter” Function: I. Characterization of Ion Fluxes

Magdalena Juhaszova ^{1,‡}, Evgeny Kobrinsky ^{1,‡}, Dmitry B. Zorov ^{1,2,‡}, H. Bradley Nuss^{1,†}, Yael Yaniv ^{1,†}, Kenneth W. Fishbein ³, Rafael de Cabo ⁴, Lluís Montoliu⁵, Sandra B. Gabelli ^{6,7,8}, Miguel A. Aon ^{1,4}, Sonia Cortassa ¹, Steven J. Sollott ^{1,*}

¹Laboratory of Cardiovascular Science, National Institute on Aging, NIH, Baltimore, MD 21224, USA, ²A.N. Belozersky Institute of Physico-Chemical Biology, Lomonosov Moscow State University, 119992, Moscow, Russia, ³Laboratory of Clinical Investigation, National Institute on Aging, NIH, Baltimore, MD 21224, USA, ⁴Translational Gerontology Branch, National Institute on Aging, NIH, Baltimore, MD 21224, USA, ⁵National Centre for Biotechnology (CNB-CSIC), Biomedical Research Networking Center on Rare Diseases (CIBERER-ISCI), 28049, Madrid, Spain, ⁶Department of Medicine, Johns Hopkins University School of Medicine, Baltimore, MD 21205, USA, ⁷Department of Oncology, Johns Hopkins University School of Medicine, Baltimore, MD 21205, USA and ⁸Department of Biophysics and Biophysical Chemistry, Johns Hopkins University School of Medicine, Baltimore, MD 21205, USA

*Address correspondence to S. J. S. (e-mail: sollotts@mail.nih.gov)

[†]Present address: Center for Scientific Review, NIH, Bethesda, MD, USA

[‡]Present address: Biomedical Engineering Faculty, Technion-IIT, Haifa, Israel

[§]Co-first author.

Preprint of this paper is available in bioRxiv: Version 2, April 22, 2019, <https://doi.org/10.1101/355776>.

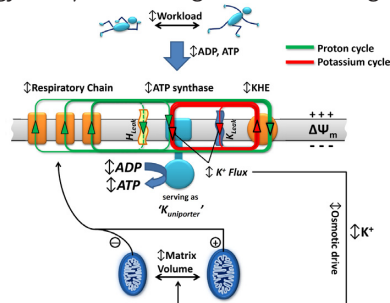
Abstract

ATP synthase (F₁F_o) synthesizes daily our body's weight in ATP, whose production-rate can be transiently increased several-fold to meet changes in energy utilization. Using purified mammalian F₁F_o-reconstituted proteoliposomes and isolated mitochondria, we show F₁F_o can utilize both ΔΨ_m-driven H⁺- and K⁺-transport to synthesize ATP under physiological pH = 7.2 and K⁺ = 140 mEq/L conditions. Purely K⁺-driven ATP synthesis from single F₁F_o molecules measured by bioluminescence photon detection could be directly demonstrated along with simultaneous measurements of unitary K⁺ currents by voltage clamp, both blocked by specific F_o inhibitors. In the presence of K⁺, compared to osmotically-matched conditions in which this cation is absent, isolated mitochondria display 3.5-fold higher rates of ATP synthesis, at the expense of 2.6-fold higher rates of oxygen consumption, these fluxes being driven by a 2.7:1 K⁺: H⁺ stoichiometry. The excellent agreement between the functional data obtained from purified F₁F_o single molecule experiments and ATP synthase studied in the intact mitochondrion under unaltered OxPhos coupling by K⁺ presence, is entirely consistent with

Submitted: 7 October 2021; Revised: 6 December 2021; Accepted: 7 December 2021

Published by Oxford University Press on behalf of American Physiological Society 2021. This work is written by (a) US Government employee(s) and is in the public domain in the US.

K^+ transport through the ATP synthase driving the observed increase in ATP synthesis. Thus, both K^+ (harnessing $\Delta\Psi_m$) and H^+ (harnessing its chemical potential energy, $\Delta\mu_H$) drive ATP generation during normal physiology.



Key words: mitochondrial K^+ transport; mitochondrial K_{ATP} channel; single molecule bioenergetics; unitary K^+ currents; proteoliposomes; ATP synthesis

Introduction

The family of ATPases shares a number of proteins with conserved functions and molecular composition.¹ F_1 -, A - and V -ATPases are true biological rotary engines that work as coupled motors: the $F_1/A_1/V_1$ is chemically driven (i.e., effecting transduction of mechanical and chemical energy) and the membrane-embedded $F_0/A_0/V_0$ is powered by the energy stored in a transmembrane ion gradient.^{2,3} Of these, a specialized group, the ATP synthases, is the major route to ATP synthesis. One of the best characterized members of ATPases is the F_1F_0 -ATP synthase (F_1F_0) of *E. coli*, mitochondria and chloroplasts. It was demonstrated that both F_1 and F_0 subunits are required for ATP synthesis.⁴

ATP synthase operates as two rotary stepper generators coupled by a common shaft, the γ subunit.⁴⁻⁶ The torque that is generated by ion flow through the F_0 motor operates against the counter-torque in F_1 driven by the energy of ATP hydrolysis. The direction of F_1F_0 is determined by which torque is larger: that of the driving force of the ion electrochemical potential or that produced by the ATP chemical potential. Under physiological conditions, F_0 torque exceeds the F_1 -generated counter-torque at ambient ATP levels, and thus the system proceeds toward ATP synthesis. Although the principal function of the F_1F_0 is to harness the energy stored in electrochemical ion gradients to make ATP, it can nevertheless run backwards (as an ATP hydrolase) pumping ions in the opposite direction in the absence of the activity of a regulated inhibitory protein. This scenario would occur if, (1) the ATP levels would rise substantially relative to the ion gradient magnitude, or (2) the ion gradient becomes dissipated, as occurs during ischemia.

Most ATPases harness the free energy of the transmembrane electrochemical proton gradient, $\Delta\mu_H$, but some use a Na^+ gradient instead (e.g., see⁷). While the mechanistic basis of ion-selectivity of various ATP synthases is a matter of considerable interest,⁸ it is even more intriguing to consider the possible significance for mitochondrial function of the accompanying “non-specific” ion flux via F_1F_0 . The specificity of F_1F_0 for H^+ over other cationic species was found to be extremely high (estimated $> 10^7$).⁹ It can be calculated using the Goldman-Hodgkin-Katz equation¹⁰ that for H^+ selectivity values of 10^7 and 10^8 , F_1F_0 would conduct a non-trivial ~ 24 and $2 K^+$, respectively, for every $100 H^+$ during normal ATP synthesis (at cytosolic pH = 7.2 and $K^+ = 140$ mEq/L) due to the $> 10^6$ -fold excess of cytoplasmic K^+ over H^+ . Given the large electrical force driving K^+ to the mitochondrial matrix, it would make sense to harness this

energy to generate ATP rather than to dissipate $\Delta\mu_K$ as heat. Because the activity of the respiratory chain is known to be regulated by intramitochondrial volume controlled by K^+ influx,¹¹ the added benefit would be the direct coupling of respiratory chain activity and $\Delta\Psi_m$ dissipation (caused by energy utilization/production) to an osmotic signal given by the amount of K^+ traversing F_1F_0 to make ATP, facilitating the proportional matching between energy supply and demand. Finally, that part of the proton gradient and energy not being directly dissipated via ATP synthase because of the equivalent movement of charge as K^+ would then be available to drive K^+ efflux from mitochondria using the K^+/H^+ exchanger (KHE), thus restoring osmotic balance. These principles are fully compatible with Mitchell’s chemiosmotic mechanism.^{12,13}

We investigated the possible existence of a novel, regulated function set for ATP synthase based on the postulated ability to harness energy from K^+ flux. This would enable K^+ uniporter-like function and serve to facilitate energy supply-demand matching, while under certain circumstances, also to function as a mK_{ATP} (see Juhaszova et al.¹⁴). The evidence presented provides direct proof of K^+ (acting together with H^+) driven ATP synthesis by F_1F_0 occurring naturally under physiological pH and K^+ concentration.

Results

Potassium Channel Openers Activate K^+ Flux into Proteoliposome-Reconstituted ATP Synthase

First, to measure K^+ flux into proteoliposome (PL)-reconstituted purified F_1F_0 (see Figure S1), the K^+ -sensitive fluorescent dye, PBFI, was trapped inside the vesicles under conditions shown in Figure 1A. In the presence of the protonophore FCCP (to enable charge balance necessary for K^+ flux and to maintain membrane potential, $\Delta\Psi_m = 0$), the K^+ channel opener (KCO) diazoxide (Dz) significantly enhanced the initial rate of K^+ flux into PL; this effect was completely blocked both by the F_0 inhibitor venturicidin B (Vent), and the mK_{ATP} blocker, 5-hydroxydecanoate (5-HD), while it was essentially absent when the endogenous regulator of ATP synthase, IF_1 was depleted from F_1F_0 PL (Figure 1B)(see also Methods section).

The reconstituted purified F_1F_0 subjected to a transmembrane K^+ gradient at $\Delta pH = 0$ generated a stable $\Delta\Psi_m$, reaching a maximal voltage of ~ 55 mV (Figure 1C). The fact that this

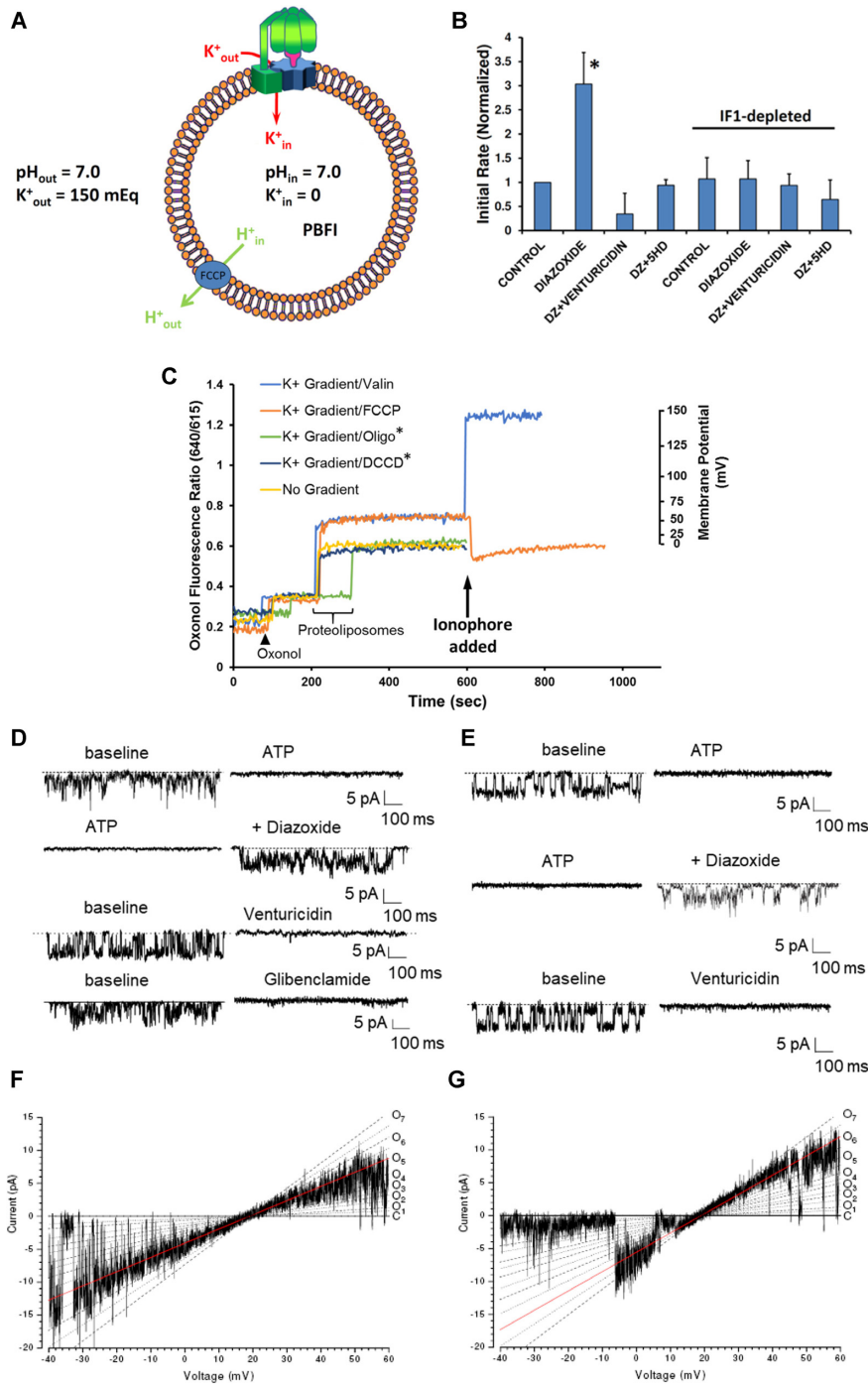


Figure 1. (A) Scheme of the proteoliposome (PL) system; ionic composition of the internal and external buffer, used in K^+ transport experiments. (B) Kinetics of K^+ flux into PL; effect of IF_1 depletion. The KCO, Dz, significantly enhanced the rate of K^+ flux into PL, this effect was blocked both by the F_0 inhibitor, Vent, and the mK_{ATP} blocker, 5-HD, and was absent in IF_1 -depleted F_1F_0 . * $P < 0.05$. (C) Ratiometric fluorescence measurements of $\Delta\Psi$ generated in F_1F_0 -reconstituted proteoliposomes by a K^+ gradient performed with oxonol VI (excitation 560, emission 640/615 nm). PL-reconstituted F_1F_0 develops a stable, non-zero K^+ diffusion-potential ($\Delta\Psi \sim 55$ mV; orange and light blue traces) in a K^+ concentration gradient (200 mM K^+ out/0.5 mM K^+ in; other conditions as in panel A except PBF1 omitted) that was completely dissipated by 1 μ M FCCP (orange trace). Addition of 10 nM valinomycin (instead of FCCP) resulted in a maximal K^+ permeability and increase of the oxonol VI fluorescence ratio representing a membrane potential of ~ 150 mV (light blue trace). F_0 inhibitors DCCD and Oligo (*PL were preincubated with each drug for 15 min; green and dark blue traces) prevented the development of $\Delta\Psi$ by the K^+ gradient; thus, ATP synthase (and not some other contaminating K^+ conductance/channel) is responsible for $\Delta\Psi$ under control conditions because it is K^+ -permeable. PL without a K^+ -gradient do not develop $\Delta\Psi$ (yellow trace). The Nernst potential-calibrated values of $\Delta\Psi$ were set by different K^+ gradients using 10 nM valinomycin (right Y-axis). (D-G) Planar lipid bilayer experiments. (D) Unitary K^+ currents from purified F_1F_0 and (E) from conventional mitochondrial membrane preparation (at -40 mV), reconstituted into lipid bilayers; pre-intervention baseline recordings are on the left, and the effect of the various compounds are shown (2 mM MgATP, 30 μ M Dz, 4 μ M Vent, 50 μ M Glib). KCOs reverse ATP-inhibited permeation of F_1F_0 by K^+ that can be blocked by Vent and Glib. (F, G) Unitary K^+ currents elicited in response to a voltage ramp (14.1 mV/sec) distinguish multiple conductance levels represented by O_1 - O_7 (C-closed state). The 216 pS conductance (O_5) is predominantly active in the recording shown in panel (F), while the 293 pS conductance (O_6) is active during the recording in panel (G) (highlighted by red lines).

$\Delta\Psi_m$ remains stable until being dissipated by FCCP, in principle, rules out the possibility of contamination by an unidentified K^+/H^+ antiport or another charge-exchange mechanism. To further elucidate this possibility, we utilized an electrophysiological approach to rule out the presence of any other cation-selective channel activity in our F_1F_0 preparations (Figure S2A and B). It has been suggested that a mitochondrial ROMK potassium channel might act as the pore-forming subunit of a cytoprotective mK_{ATP} channel.¹⁵ Our immunoblotting with anti-ROMK antibody ruled out ROMK channel contamination of the isolated F_1F_0 (Figure S2C).

Measurement of Unitary K^+ and H^+ Currents from F_1F_0

In unitary ion channel recordings from lipid-bilayer reconstitution experiments with purified F_1F_0 , Dz reversed ATP-inhibited ion flux that can be blocked by the F_0 inhibitor, Vent, by the mK_{ATP} inhibitor, glibenclamide (Figure 1D and Supplemental Movie S1) and by F_0 inhibitors oligomycin and N, N'-dicyclohexylcarbodiimide (DCCD; see below). Considering that similar findings are obtained in conventional mitochondrial membrane reconstitution studies (i.e., without using a purified F_1F_0), for the first time, to our knowledge, we show that the unitary ion currents derived from conventional mK_{ATP} preparations, which display the same characteristics as the purified F_1F_0 complex, can be largely inhibited by Vent (Figure 1E) at levels that do not affect sarcolemmal K_{ATP} currents. Unitary currents from purified F_1F_0 exhibit multiple conductance levels as shown in Figure 1F,G and is clearly seen in the full time series at Supplemental Movie S1 in agreement with single channel behavior of conventional mK_{ATP} preparations. Note that the adoption of the multiple discrete conductance levels shows stochastic behavior manifesting a variety of long and short open-closed dwell times; the "high-frequency" events represent true, "channel-like" gating and not bilayer noise (Supplemental Movie S1). This complex behavior may arise from the multiple ion-binding positions on the F_0 c-ring. A comprehensive literature search regarding the single channel characteristics of conventional mK_{ATP} channel preparations reconstituted into lipid bilayers indicates that multiple levels are frequently observed (five distinct peaks/conducting states between 20 pS and 120 pS in symmetric 150 mM K glutamate^{16,17} and conductances between 10 and 200 pS in symmetric 100 mM KCl,^{18,19} which is largely consistent with the present data.

The ion-specificity of the observed unitary currents requires closer examination because mammalian F_1F_0 is thought to make ATP only by H^+ flux. In the present experiments, the abundance of K^+ over H^+ was $\sim 10^6:1$ (comparable to that occurring in cells), so it is reasonable to consider that K^+ permeation may be contributing as well. Furthermore, the potential contribution of anion permeation cannot be excluded a priori. Because only permeant ions contribute to the net ion-current reversal potential (E_{rev}), this was examined in detail under various conditions to assess the possibility of anion permeation and to interpret the changes in cation permeation activated by KCOs. Since complete substitution of the substantially larger and rather non-permeant Hepes anion for Cl^- causes no change in E_{rev} (17.9 ± 0.7 vs 18.6 ± 0.5 mV, respectively, $P = ns$), we concluded that the impact of Cl^- permeation via F_1F_0 is insignificant compared to cations. Additionally, the current-voltage relationship of purified F_1F_0 was examined in a pH gradient ($pH_{cis} = 8.0$, $pH_{trans} = 7.2$, buffered by TEA^+ -Hepes, in the absence of K^+ or any other small cation aside from H^+) yielding a reversal potential identical to the expected

Nernst potential for H^+ as the only permeant species, in agreement with the idea that the OH^- anion is non-permeant. Since the measured unitary ion currents under control conditions consist only of H^+ and K^+ , we next assessed their relative contributions. Under ionic conditions where the reversal potential for H^+ (E_H) was 0 mV and that for K^+ (E_K) was +28 mV, E_{rev} was found to be $\sim +18$ mV indicating that both cations must be permeant and contributing to the total currents observed. In this case, E_{rev} is given by:

$$E_{rev} = \frac{RT}{F} \ln \left(\frac{P_K [K]_o + P_H [H]_o}{P_K [K]_i + P_H [H]_i} \right) = \frac{RT}{F} \ln \left(\frac{[K]_o + \frac{P_H}{P_K} [H]_o}{[K]_i + \frac{P_H}{P_K} [H]_i} \right) \quad (1)$$

where:

R is the molar gas constant;

F is Faraday's constant;

T is temperature ($^{\circ}K$);

P_K and P_H are the respective ion permeabilities;

$[K]_{o,i}$ and $[H]_{o,i}$ are ion concentrations across the bilayer

Maintaining steady voltages at each of the ion-reversal potentials (to remove the driving force from the specific cation, thus rendering pure unitary current from the other cation) produced macroscopic H^+ and K^+ currents (at +28 and 0 mV, respectively) of the same characteristics and open probability (P_o) as at -20 or -40 mV (Figure 1F and G). Importantly, the KCO Dz increases P_o and amplitude for both H^+ and K^+ currents (Figure 1D and E) without causing any change in E_{rev} (18.3 ± 1.3 vs 18.5 ± 0.9 mV with Dz, $P = ns$; similar data was obtained with Na^+ : 18.1 ± 1.0 vs 18.9 ± 1.0 mV; $n = 10$). This indicates that while the permeability for H^+ and K^+ after Dz increases for both cations, the ratio (P_H/P_K) remains unchanged (see eq. 1). From the Goldman-Hodgkin-Katz (GHK) formalism, the total ion current is related to the individual ion permeability as follows:

$$I = P_H Z_H^2 \frac{VF^2}{RT} \left(\frac{[H]_i - [H]_o \exp\left(\frac{-Z_H VF}{RT}\right)}{1 - \exp\left(\frac{-Z_H VF}{RT}\right)} \right) + P_K Z_K^2 \frac{VF^2}{RT} \left(\frac{[K]_i - [K]_o \exp\left(\frac{-Z_K VF}{RT}\right)}{1 - \exp\left(\frac{-Z_K VF}{RT}\right)} \right) \quad (2)$$

where:

Z is the appropriate ion valence;

V is the transmembrane voltage

We determined that the baseline values for P_H and P_K ($5.2 \pm 0.9 \times 10^{-11}$ and $8.7 \pm 2.9 \times 10^{-17}$ m^3/s , respectively) each increases ~ 3.5 -fold after Dz (to $2.2 \pm 1.3 \times 10^{-10}$ and $3.0 \pm 1.4 \times 10^{-16}$ m^3/s , respectively, $n = 4$, both $P < 0.05$ vs. each ion's baseline value), thus keeping the selectivity of F_1F_0 for H^+ over K^+ at $\sim 10^6:1$. Regarding the single ion channel behavior of the conventionally-prepared mK_{ATP} , close inspection of the electrophysiological data referred in eight published papers allowed us to extract baseline values for P_H and P_K (mean values of $4.9 \pm 1.1 \times 10^{-11}$ and $1.9 \pm 0.5 \times 10^{-16}$ m^3/s , respectively)²⁰⁻²⁷ which compare extremely well with those obtained here for F_1F_0 .

The importance of F_1F_0 as a major K^+ pathway can be realized from Eq. 2 which shows the sum of the K^+ and H^+ current components in the GHK formulation. For sufficiently large $\Delta\Psi_m$ magnitudes (>100 mV for the present case), a rearrangement of Eq. 2 expressing the ratio of K^+ to H^+ conducted by F_1F_0 simplifies to the limiting value, $[(P_K [K^+]_{cytosol}) / (P_H [H^+]_{cytosol})]$ at negative $\Delta\Psi_m$ (the direction of ATP synthesis). Thus, during normal ATP

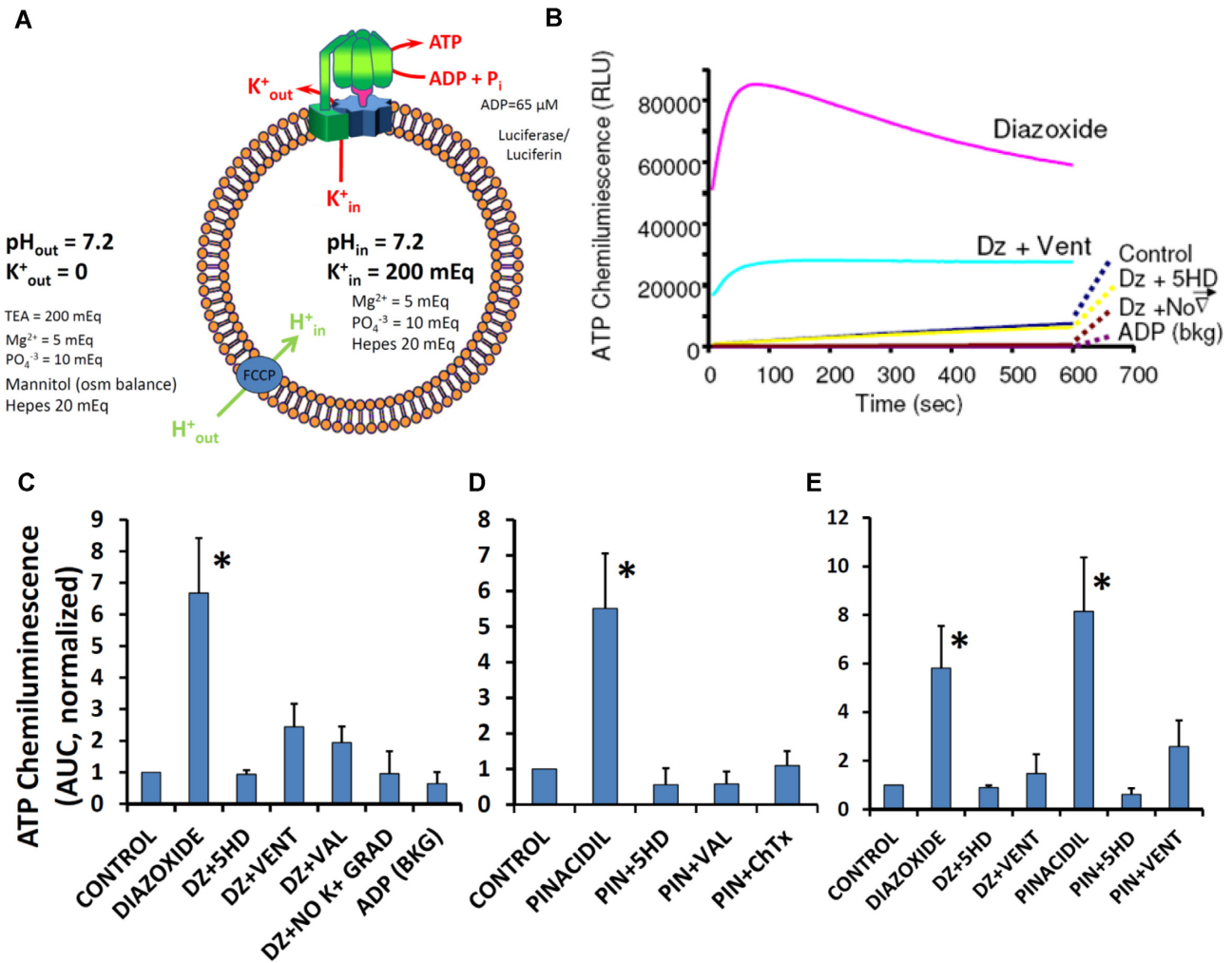


Figure 2. (A) Scheme of the PL and reaction conditions to measure K^+ transport-coupled ATP synthesis (and hydrolysis). $\Delta\mu_H = 0$ for ATP synthesis and $\Delta\Psi = 0$ by using FCCP; n.b., omitting FCCP eliminates ATP synthesis ruling out the presence of an unsuspected, underlying K^+/H^+ antiport mechanism. (B, C) K^+ -gradient-driven ATP production in PL is activated by Dz and (D) pinacidil, and (B–D) attenuated by inhibitors of F_1F_0 , inhibitors of the mK_{ATP} and BK_{Ca} channels, and by K^+ gradient dissipation (Val or No K^+ grad). (E) Na^+ -gradient-driven ATP production in PL is activated by Dz and pinacidil and attenuated by inhibitors of complex V and the mK_{ATP} (performed as in panel (A) except equimolar concentration of Na^+ substituted for K^+). These experiments prove that the entity activated by KCOs is the F_1F_0 . * $P < 0.05$.

synthesis (cytosolic $pH = 7.2$ and $K^+ = 140$ mEq/L), F_1F_0 may potentially conduct an average of 3.7 K^+ for every H^+ . Under these conditions, K^+ influx into mitochondria used by F_1F_0 for ATP production would depend solely on $\Delta\Psi_m$ because of its magnitude (i.e., exponential term in Eq. 2) and not on ΔK^+ across the inner membrane, nor on matrix K^+ concentration (i.e., linear term in Eq. 2, dwarfed by the exponential term; for further explanation, see section: Quantitative comparison of H^+ and K^+ current magnitudes through ATP synthase in Supplemental information).

ATP Synthesis by Proteoliposome-Reconstituted F_1F_0 in a K^+ Gradient

To investigate whether ATP synthase can harness energy from K^+ -flux, purified F_1F_0 reconstituted into PL was subjected to a transmembrane K^+ gradient (Figure 2A). Under conditions in which $\Delta\Psi = 0$, and $\Delta\mu_H$ and H^+ were unable to drive ATP synthesis due to the presence of protonophore, FCCP, we show that ATP synthesis driven by the K^+ gradient occurs under these conditions, and was increased several-fold by the KCOs, Dz or

pinacidil. This ATP synthesis was inhibited by the specific F_0 inhibitor, Vent, the mK_{ATP} blocker, 5-HD, and abolished by the K^+ ionophore, valinomycin (Val) (Figure 2B–D). Interestingly, the F_1F_0 is not selective among alkali ions after KCO-activation, since we observed a comparable degree of ATP synthesis in a Na^+ gradient, akin to that in a similar K^+ gradient (Figure 2E). Moreover, this effect seems to be restricted to small cations, since there is no ATP generated by KCO activation of the F_1F_0 in a comparable gradient of TEA^+Cl^- . Similar K^+ gradients with either Cl^- or SO_4^{2-} as counterions yielded comparable ATP amounts (not shown). It is important to note that FCCP is necessary to enable ATP synthesis driven by the K^+ gradient because it equilibrates the transmembrane charge (via passive inward diffusion of H^+) owing to $\Delta\mu_K$ -driven K^+ efflux via F_1F_0 . Omitting FCCP eliminates ATP synthesis ruling out the possible contamination of the PL's by an unsuspected protein which might cause an underlying K^+/H^+ antiport activity (also see section, Potassium channel openers activate K^+ flux into proteoliposome-reconstituted ATP synthase, Figure 1C and Figure S2 for additional details). Thus, any possibility that the observed ATP synthesis was due to F_1F_0 surreptitiously harnessing H^+ flux energy

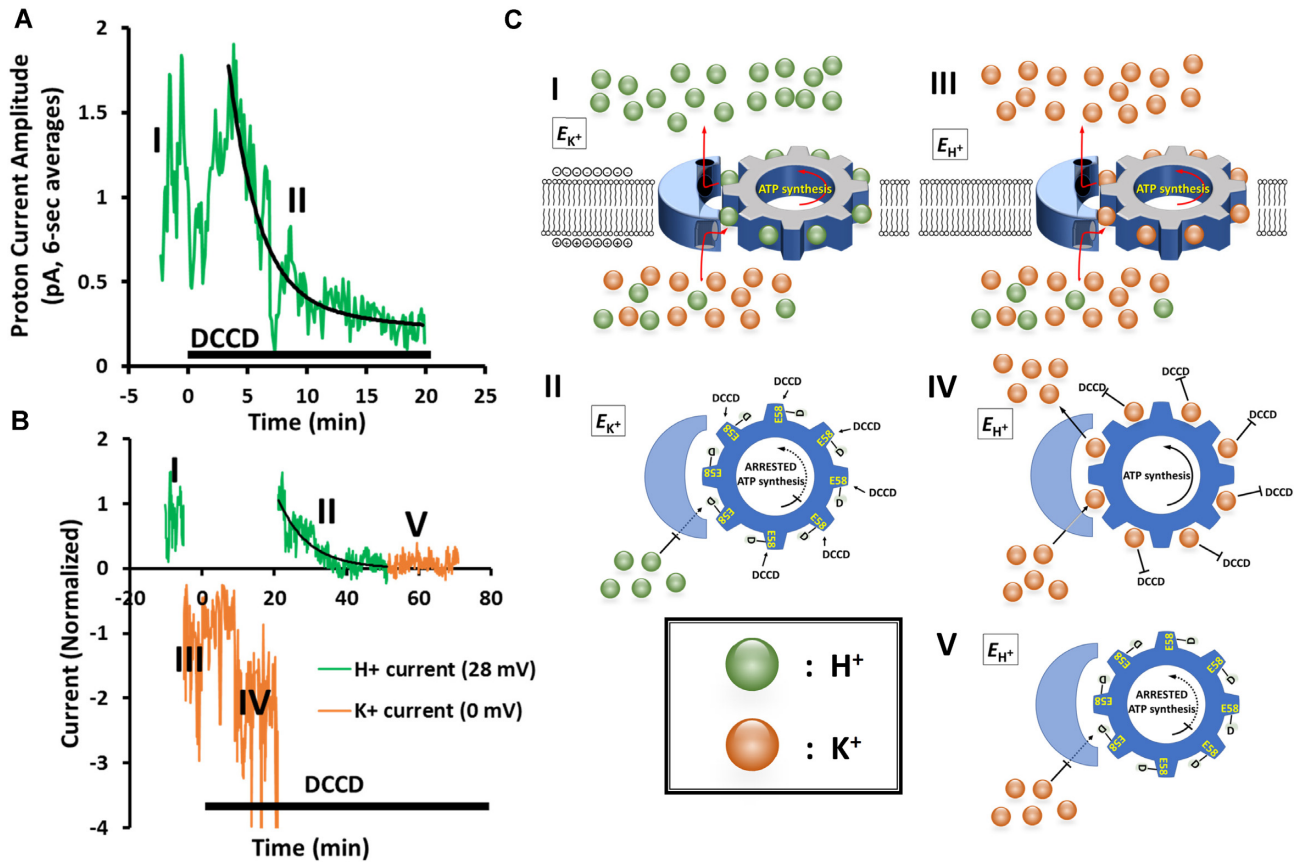


Figure 3. Effect of DCCD on lipid bilayer-reconstituted F_1F_0 activity during conduction of pure H^+ (at +28 mV, green traces) and K^+ (at 0 mV, orange traces) currents (cis: 150 mEq/L K^+ , pH 7.2/trans: 50 mEq/L K^+ , pH 7.2; 1 kHz-recorded data for multiple-minute experiments are plotted as 6-sec averages). (A) Continuous recording of unitary H^+ current (phase "I"; green trace); H^+ current is completely blocked by DCCD with $t_{1/2} \sim 6$ min (phase "II"; exposure to DCCD is indicated by the black horizontal bar). (B) Baseline performance of F_1F_0 initially driven by H^+ current (phase I; green), then switched to K^+ current (phase "III," orange), followed by addition of DCCD (black bar, initiated at "0" time) which fails to block K^+ current-driven activity after 20 min (phase "IV," orange), then switched back to H^+ current (at 20 min DCCD exposure, phase "II," green) leading to rapid inhibition of activity, then back to K^+ current (at 50 min DCCD, phase "V," orange) displaying persistence of inhibition. (C, Panels I-V) Mechanistic schema of "phases" of F_1F_0 driven by K^+ (orange) or H^+ (green) currents corresponding to those depicted in panels A, B. (C_I) H^+ -driven rotation at the reversal potential for K^+ (E_{K^+}); (C_{II}) inhibition of H^+ -driven rotation after DCCD reaction with protonated E58; (C_{III}) K^+ -driven rotation at the reversal potential for H^+ (E_{H^+}); (C_{IV}) inability of DCCD to inhibit K^+ -driven rotation due to occupancy of E58 by K^+ (rather than by a H^+ required for DCCD reaction and formation of the acylurea adduct); (C_V) once the enzyme is deactivated by DCCD during prior H^+ current passage (and formation of a stable acylurea adduct on E58), subsequent K^+ flux is also blocked. Together, these results serve as another line of proof that mammalian F_1F_0 can operate utilizing K^+ flux, and that both K^+ and H^+ travel the same route within the complex on the c-ring.

(somehow derived from the original K^+ gradient energy) is ruled out by this FCCP result, because ATP synthesis would instead have been prevented by the protonophore-elicited dissipation of H^+ energy. This evidence also shows that K^+ can drive ATP synthesis by the same mechanism and path as H^+ .

To further investigate whether the K^+ and H^+ paths through F_1F_0 are the same, we utilized the inhibitor DCCD that acts by specifically and covalently modifying the protonated form of a conserved glutamate carboxylate (in mammalian c-ring E58) located in the binding pocket of the membrane-embedded c-ring²⁸⁻³⁰ and performed measurement of unitary ion channel currents from F_1F_0 under conditions where we could generate and select pure K^+ and H^+ currents by setting specific membrane potentials. Since E58 is critical for coordinating ion binding necessary for the H^+ gradient to generate ATP, we found that DCCD rapidly inhibits ion flux ($t_{1/2} \sim 6$ min) when being driven by pure H^+ current (Figure 3A, C_{I,II}), as expected. So long as the c-ring binding pockets are H^+ -bound, continuing active H^+ flux is not required for DCCD's block since we found that the inhibition fully develops when the c-ring is "stalled" without ion flow after running pure H^+ current (Figure S3).

We hypothesized that E58 in the deprotonated state is also critical for K^+ binding related to its generation of ATP, and that occupancy of the same binding site by K^+ (likely by preventing glutamate protonation via charge neutralization and physical exclusion) would specifically prevent F_1F_0 from reacting with, and being inactivated by, DCCD (Figure 3B, C_{III,IV}). We employed K^+ -only current conditions (i.e., under the present experimental conditions at 0 mV where there is no H^+ driving force, and hence, no H^+ current) for 5 min before exposure to DCCD (Figure 3B orange trace labelled "III," and Figure 3C_{III}). We found that the maintenance of K^+ -flux and binding prevented the subsequent DCCD block for at least 15 min (Figure 3B, orange trace labelled "IV," and Figure 3C_{IV}), and for as long as 1 hour under continuous K^+ currents (Figure S3), indicating protection of E58 by K^+ from the inhibitory reaction with DCCD. Similar protection by Na^+ from inhibition by DCCD was described for this conserved, essential Glu site of the c-subunit from *P. modestum*²⁸. Returning to driving F_1F_0 with H^+ currents after the "protective" K^+ current protocol, in the continuing presence of DCCD, lead to rapid and irreversible inhibition of the enzyme (Figure 3B green trace labelled "II," Figure 3C_{II}, and Figure S3). Once the enzyme

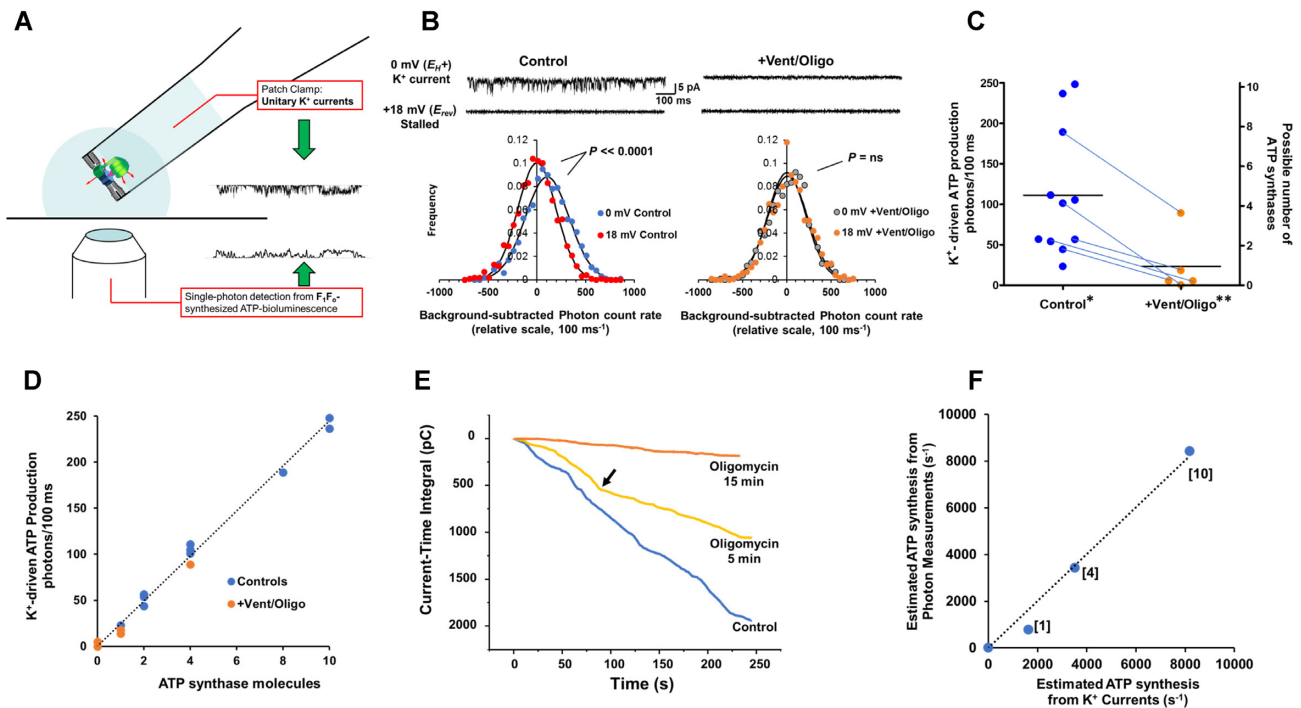


Figure 4. Direct, “single molecule bioenergetics” demonstration of K⁺-driven ATP synthesis by F₁F₀ using simultaneous measurements of K⁺ currents and single-photon detection of ATP. (A) Experimental scheme for simultaneous measurements of unitary K⁺ currents (by voltage clamp) and low light level detection of ATP synthesis activity (luciferase/luciferin bioluminescence) from reconstituted single molecules of F₁F₀ in a lipid bilayer formed on a 30–50 μm glass pipette (cis: 150 mEq/L K⁺, pH 7.2/trans: 50 mEq/L K⁺, pH 7.2). (B) Representative experiment performed as described in (A). Top traces: K⁺ current in control (left) and that after F₁F₀ inhibition by Vent + Oligo (right), together with corresponding measurements with F₁F₀ activity stalled at E_{rev}. Bottom panels: Frequency histograms of detected bioluminescence photons from ATP generated by K⁺-driven F₁F₀ (background-subtracted photon counts measured during K⁺ current (0mV) and at the E_{rev} (18mV); Control experiment (left) vs Vent + Oligo block (right)). Note that the Control photon-rate frequency histogram during active K⁺ currents (at 0 mV, E_{H+} vs E_{rev}; n = 1000 observations each histogram, $P << 0.0001$ for paired comparison), and that both the 0 mV current and associated photon production are abolished with + Vent/Oligo (E_{H+} vs E_{rev}; n = 1000 observations each histogram, $P = ns$). (C) Concatenated experimental results: K⁺-driven photon production in control (0 mV vs stalled at +18mV, n = 11 paired observations, $*P << 0.0001$ by Fisher’s combined probability test) and that after F₁F₀ inhibition by Vent + Oligo (paired observations with control, n = 5, $**P << 0.0001$ by Fisher’s combined probability test); measured photon production rates from K⁺-driven ATP synthesis appeared to be quantized in relation to the number of incorporated F₁F₀ (“Possible number of ATP synthases” on right y-axis; see text for further details). (D) Analysis of apparent quantal nature of K⁺-driven photon (ATP) production rate vs the proposed number of bilayer-incorporated ATP synthase molecules (from experimental results, panel (C)); regression analysis slope of ~25 photons/100 ms/ATP synthase, $R^2 = 0.99$. (E) Evidence for F₁F₀ lipid bilayer insertions as functional dimers. Time course of the cumulative K⁺ current-time integral recording (running ATP synthesis index) from a representative F₁F₀ experiment in control (blue trace) and during Oligo inhibition (yellow and orange traces); arrow (yellow trace, 5 min Oligo) indicates abrupt change of the current-time integral slope (to half of the control value) consistent with the initial activity of an F₁F₀ dimer being reduced by one functional unit to the equivalent of a monomer; after 15 min Oligo (orange trace), the activity of the remaining F₁F₀ (monomer) becomes fully inhibited (n.b., slight deviation from a zero-slope is a typical baseline artifact of cumulative electrical drifts in 4 + minute electrical recordings, and because it occurs in lipid bilayer recordings without protein incorporation, does not represent residual ATP synthase activity). (F) Relationship between ATP synthesis rates calculated from single photon vs K⁺ current measurements (see text for details). The number of F₁F₀ molecules is shown in brackets for several independent experiments; the average ATP synthesis rate is ~1000 ATP/sec/F₁F₀ driven solely by K⁺ current in the nominal absence of ATP (thus without significant counter-torque on F₁, in contrast to physiological conditions). ATP synthesis rates estimated independently from single photon vs K⁺ current measurements are in excellent agreement, deviating from unity by < 18%, $R^2 = 0.98$.

was deactivated by DCCD during H⁺ current passage, we found that K⁺ flux is also blocked (Figure 3B orange trace labelled “V” and Figure 3C_V; Figure S3), consistent with the DCCD reaction forming a stable acylurea adduct on E58. Together, these results serve as another line of proof that mammalian F₁F₀ can operate utilizing K⁺ flux, and that both K⁺ and H⁺ travel the same route within the complex on the c-ring.

Direct Demonstration of K⁺-Driven ATP Synthesis by Simultaneous Measurements of K⁺ Currents and Single-Photon Detection of ATP: “Single Molecule Bioenergetics”

To directly demonstrate that ATP synthesis can be driven specifically by K⁺ flux through F₁F₀ and the energy stored in an electrochemical K⁺ gradient, we designed a unique system for simul-

taneous measurement of unitary K⁺ ion currents (by voltage clamp) together with ATP synthesis (from low light-level detection of bioluminescence) generated by single molecules of ATP synthase (Figure 4). Single molecules of purified F₁F₀ were reconstituted in the lipid bilayer formed on a 30–60 μm glass pipette tip (Figure 4A). Pure K⁺ current-driven ATP synthesis activity due to Δμ_K produced by the experimental K⁺ gradient (at 0 mV, when Δμ_H = 0) was accompanied by a significant increase in the photon rate (i.e., real ATP generation) over background (at 18 mV with F₁F₀ stalled and no K⁺ or H⁺ currents) that in turn was significantly inhibited by specific F₀ blockers, Vent/Oligo (representative experiment in Figure 4B; concatenated results in Figure 4C). This experiment provides unambiguous and definitive proof of K⁺-driven ATP production by single molecules of mammalian ATP synthase under conditions reasonably matching the physiological K⁺ ionic milieu. In this experiment, K⁺, the only monovalent cation capable of performing electrochemical work, is thermodynamically

driven by its preset gradient in the direction of ATP synthesis, whereas protons are incapable of performing work because the experiment is performed under circumstances constraining $\Delta\mu_{\text{H}} = 0$. That the entity that synthesizes ATP as a result of the work performed by K^+ flux is significantly blocked by the specific F_0 inhibitors, Vent and Oligo, provides corroborating proof that ATP synthase is responsible for the observed synthesis of ATP, and not some unknown (or undescribed) complex.

The range of measured photon production rates from these experiments varied by an order of magnitude (~25 to 250 photons/100 ms) and appeared to be quantized (allowing for “noise”) with a “greatest common factor” of ~25 photons/100 ms which is probably consistent with the activity of 1 monomer of ATP synthase (Figure 4C right y-axis, D). We expected that there could be occurrences of multiple ATP synthases since these latter experiments were prepared with an increased amount of purified F_1F_0 intended to increase both the potential for multiple insertions of ATP synthase into the lipid bilayer and the detected bioluminescence signal over noise. Plotting the K^+ -driven photon production rate vs the proposed number of ATP synthase molecules (from 1 to 10 ATP synthases), and performing regression analysis of all experimental results, rendered a slope of ~25 photons/100 ms/ATP synthase (Figure 4D). The data pattern suggests that most of the insertions observed are of ATP synthase dimers and multiples thereof, whereas isolated monomers appeared to be relatively rare (accounting for < 10% of observed occurrences). There are several additional lines of evidence for the idea of ATP synthase dimer-insertions: (i) examining the time course of inhibition of K^+ current flux by oligomycin to find a quantal pattern of inhibition. In experiments producing ~50 photons/100 ms at baseline (indicated as dimers in Figure 4C) the current-time integral (CTI, the precise “electrical analog” of cumulative ATP synthesis) shows in a representative example that at ~5 min of oligomycin exposure the time-dependent slope of CTI (proportional to ATP synthesis rate) is abruptly reduced by exactly half, consistent with the activity of a dimer being reduced by one functional unit to the equivalent of a monomer (Figure 4E, yellow trace, arrow), and subsequently, after 15 min, the activity of the remaining ATP synthase becomes fully inhibited (Figure 4E, orange trace). (ii) Purified ATP synthase is isolated mainly as dimers in the current protocol, as gauged by the abundance of ATPase activity in Clear Native PAGE in-gel assay (Figure S1). (iii) ATP synthases form rows of natural dimers along cristae in mitochondria (e.g., as shown in five different species: bovine, *Y. lipolytica*, *P. anserina*, *S. cerevisiae*, and potato)³¹ and are isolated as natural dimers by other workers (e.g., as shown using transmission electron microscopy).³²

We sought to further quantify and compare the ATP synthesis rates independently derived from single molecule electrical and bioluminescence measurements. Bioluminescence-emitted photon measurements, concatenated with the efficiencies of the ATP-luciferase reaction, light path and camera detection characteristics, together with the fraction of the solid angle collected from an isotropically emitting point source by the objective lens, produce a quantitative estimate of ATP production rate (see Supplementary Methods). Additionally, an independent estimate of ATP synthesis rate from these same experiments can be derived from the parallel unitary current measurements since three ATP's are made from the flux of eight ions through mammalian ATP synthase. Excellent agreement was obtained for single molecule ATP synthesis rates calculated from photon vs K^+ current measurements incorporating the range of 1, 4 and 10 ATP synthases (<13% deviation from the line of identity; Figure 4F, $r^2 = 0.93$), yielding the consistent value of ~1,900

ATP/s/ATP synthase driven by K^+ (± 50 , SEM of $n = 11$), which is in good agreement with published data (e.g.,³³). Note that ATP synthase is operating in these experiments against a negligible counter-torque because the ambient [ATP] is negligible, which is experimentally necessary to resolve the extremely low levels of bioluminescence generated from the driven activity of single molecules of ATP synthase. In the presence of “physiological” levels of ATP (~3-4 mM) the resultant chemical counter-torque exerted at F_1 against the electrical torque driving F_0 would reduce ATP synthesis by about an order of magnitude (see section in Juhaszova et al.¹⁴ on “Regulation of mechanochemical efficiency of F_1F_0 ”), so the equivalent ATP synthesis rate in these K^+ -driven experiments would be ~190 ATP/s/ATP synthase (± 5 , SEM of $n = 11$) in an intracellular milieu, which is in good agreement with published data.³⁴⁻³⁷

K^+ -driven ATP Synthesis in Isolated Heart Mitochondria

Measurements of K^+ flux, a stable K^+ -diffusion potential, and purely K^+ -driven ATP synthesis in proteoliposome- and single molecule-reconstituted ATP synthase (Figures 1-3), together with unitary K^+ and H^+ currents sustained by purified F_1F_0 reconstituted in lipid-bilayers (Figure 1D, F, G), show that ATP synthesis can happen under physiological conditions (cytosolic pH = 7.2 and $\text{K}^+ = 140$ mEq) in which F_1F_0 is driven by up to ~3.5 K^+ for every H^+ . These findings predict that, in mitochondria, K^+ transport carried by F_1F_0 would share a sizable portion of the ATP synthesis flux driven by $\Delta\mu_{\text{H}}$ with a high $\text{K}^+ : \text{H}^+$ stoichiometry.

To assess these predictions, we studied the effect of physiological levels of K^+ on the ATP synthesis flux and the corresponding $\text{K}^+ : \text{H}^+$ stoichiometry in isolated mitochondria at constant osmolality (260 mOsm) in the presence vs absence of K^+ (isotomically substituting sucrose for K^+). We quantified the Oligo-sensitive oxygen consumption rate (OCR) with high-throughput Seahorse respirometry (Figure 5A), and ADP/O ratio with high resolution respirometry (Oroboros) (Figure 5B). At similar respiratory control ratio (RCR~5) (Figure 5E), ATP synthesis was 3.5-fold higher in the presence of K^+ than in its absence (Figure 5C) with a $\text{K}^+ : \text{H}^+$ stoichiometry of 2.7:1 (Figure 5D). More robust ATP synthesis with K^+ resulted from a 2.65-fold higher respiratory flux (Figure 5A) at ADP/O ratio 2.0 and 1.6 (Figure 5B) in the presence and absence of K^+ , respectively. Under these conditions, a significant mitochondrial K^+ influx occurs during state 4-to-3 transitions. The OCR values were within the range of reported data under similar conditions (Table S1). To further investigate the role of respiratory substrates on the ATP synthase flux in the presence or absence of K^+ , we used palmitoyl CoA (PCoA), Carnitine and malate (Mal). Similar results to G/M were obtained in the presence of these substrates. In KCl vs sucrose, 20 μM PCoA/0.5mM Carnitine/0.5mM Mal were able to sustain a 1.7-fold and 3.7-fold larger OCR and ATP synthesis flux, respectively, with a $\text{K}^+ : \text{H}^+$ stoichiometry of 2.7:1 (see Figure S5, and its legend).

Next, we employed radioactive tracers to measure the protonmotive force (PMF), and its individual components, $\Delta\Psi_{\text{m}}$ and ΔpH , in isolated rat heart mitochondria in the presence or absence of K^+ at constant (260mOsm) osmolality under states 4 and 3 respiration (Figure 5F-H). While $\Delta\Psi_{\text{m}}$ was similar under both respiratory states and in absence or presence of K^+ (Figure 5G), ΔpH was significantly higher under state 3 compared to state 4 respiration in the absence of K^+ whereas it remained constant in its presence (Figure 5H). This resulted in 0.3 pH units increase in the matrix when K^+ was absent (pH_i 8.4 vs. 8.1) (Figure 5I) with pH 7.2 in the medium. In K^+ absence, the flux

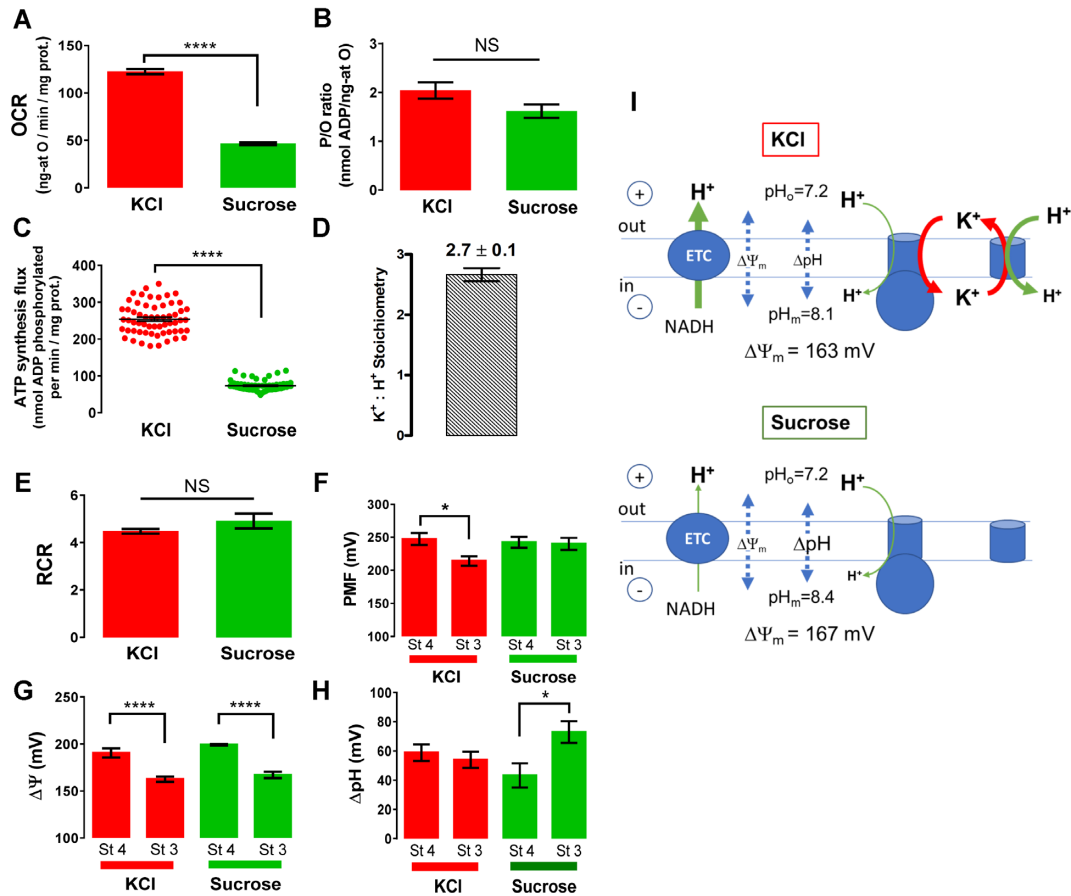


Figure 5. Respiration of isolated rat heart mitochondria. (A) Seahorse-instrument oxygen consumption rate (OCR) under state 3 was determined in KCl- or sucrose-based assay medium in the presence of 5/5mM G/M and 0.5mM ADP. The oligomycin-sensitive OCR was obtained by subtracting from state 3 OCR the state 4 OCR measured in the presence of 10 μ M oligomycin; n = 60/3 experiments, $P < 0.0001$. (B) P/O ratio was measured using high resolution respirometry as described in Methods under similar conditions as those described in panel G; n = 9/3 experiments, $P = \text{ns}$. (C) The ATP synthesis flux was calculated as the product of the oligomycin-sensitive OCR times the P/O ratio in K⁺- or sucrose-based assay medium; n = 60/3 experiments, $P < 0.0001$. (D) The K⁺/H⁺ stoichiometry was calculated from the difference between the ATP synthesis flux in the presence of KCl vs in the presence of sucrose, in ratio to the ATP flux in sucrose; n = 46/3 experiments. (E) Respiratory control ratio (RCR) was obtained from the OCR ratio state 3/state 4; n = 60/3 experiments, $P = \text{ns}$. (F) The proton motive force (PMF) was determined according to: $\text{PMF} = \Delta\Psi_m - Z\Delta\text{pH}$ using $\Delta\Psi_m$ (panel G); n = 8/3 experiments; $P < 0.0001$ and $Z\Delta\text{pH}$ (panel H); n = 8/3 experiments; $P < 0.05$ obtained under the indicated conditions with $Z = 2.303\text{RT}/F$ (see also Supplemental Experimental Procedures). (I) Summary scheme describing the ion fluxes and their respective driving forces, $\Delta\Psi_m$ and ΔpH , determined under state 3 respiration in K⁺- or sucrose-based medium (see also Supplemental Experimental Procedures). * $P < 0.05$; **** $P < 0.0001$

through the ETC is higher than through ATP synthase resulting in increased matrix alkalization. In the K⁺ media, the extra matrix alkalization is prevented due to the additional flux of K⁺ through F₁F₀ accompanied by increased ATP synthesis and enhanced H⁺ entering mitochondria through the K⁺/H⁺ exchanger (Figure 5I). Importantly, PMF, as an energy-proportional index, exhibited a significant decrease under state 3 respiration in the presence of K⁺, consistent with the additional output of ATP, whereas it remained constant in its absence (Figure 5F).

Using dynamic, simultaneous, fluorometric monitoring of $\Delta\Psi_m$, NAD(P)H and volume (90° light scattering) rather than steady state measurements, we investigated possible effects of matrix alkalization on carbon substrate oxidation during state 4→3 transition in mitochondrial suspensions subjected to the addition of ADP pulses of increasing concentration (Figure S4H-M). Under both conditions of K⁺ presence and absence, the RC flux is controlled downstream of NADH, e.g., by the RC activities, ATP synthase, etc., (i.e., the “pull” condition)^{38,39} as can be judged by the *in-phase* response of mitochondrial $\Delta\Psi_m$, NAD(P)H

and volume, as a result of the increase in energy demand exerted by the ADP pulses, ruling out a matrix alkaline-pH limitation on substrate oxidation in either condition (Figure S4H-O).

Mitochondrial volume changes associated with the state 4→3 transition, as measured with radioactive tracers, were greater in the K⁺-containing medium (1.25 ± 0.15 to 0.81 ± 0.16) than in sucrose (1.27 ± 0.19 to 1.06 ± 0.13 $\mu\text{l}/\text{mg prot}$) reflecting a more dynamic and higher rate of ADP influx and conversion to ATP, thus higher amplitude of volume changes in salt medium associated with the transition to from low to high respiration (see also Figure S4L-O). These results were corroborated by our fluorometric simultaneous measurements of $\Delta\Psi_m$ and volume of isolated heart mitochondria, where we show that, in the presence of K⁺, mitochondria exhibit significantly faster ATP synthesis as revealed by the shorter time lapse utilized to fully consume the ADP added (roughly 1000 sec vs. 1600 sec: compare H and I in Figure S4; see also panels N, O).

The existence of a substantial mitochondrial K⁺ influx, associated with ATP synthesis in mitochondria, was confirmed by

an independent, direct assessment of changes in the matrix K^+ accumulation in mitochondria loaded with the K^+ -sensitive probe PBFI. In the K^+ -based medium, a significant oligomycin-sensitive mitochondrial K^+ influx happened during the state 4-to-3 transitions (Figure S4 B, D). Thus, in the presence of K^+ , both respiratory chain and the ATP synthase are operating at higher rates which supports the notion that both H^+ and K^+ transport (with both $\Delta\mu_K$ and $\Delta\mu_H$ energies) are utilized to synthesize ATP.

Together, our data indicate that mitochondria synthesize 3.5-fold higher rates of ATP synthesis in the presence of K^+ compared to osmotically-matched conditions in which this cation is absent. The 2.6-fold higher respiratory flux is mainly responsible for the higher ATP synthesis flux driven by a 2.7:1 K^+ : H^+ stoichiometry. Thus, in the presence of K^+ , both $\Delta\mu_K$ and $\Delta\mu_H$ energies ($\Delta\mu_H$ producing $\Delta\mu_K$ almost entirely through the driving force of $\Delta\Psi_m$) are utilized to synthesize ATP with the resulting matrix-accumulated K^+ being continuously restored via the $\Delta\mu_H$ -driven K^+/H^+ exchanger (Figure 5I, top). In the absence of K^+ , ATP synthase relies only on H^+ , thus obligating a greater contribution of the ΔpH component of the PMF to ATP synthesis (as evidenced by an additional matrix alkalization of 0.3 units which is not observed in the presence of K^+) (Figure 5I, bottom; see also Discussion). The presence of any significant inner membrane K^+ leak pathway (e.g., through an unspecified channel) can be ruled out as an explanation for this K^+ influx since it would have significantly uncoupled OxPhos, lowering RCR and P/O ratio in the presence of K^+ . Instead, OxPhos coupling was unaltered by K^+ presence, and the data is entirely consistent with K^+ transport through the ATP synthase driving the observed increase in ATP synthesis. Thus, there is excellent agreement between the functional data obtained from purified F_1F_0 single molecule experiments and ATP synthase studied in the intact mitochondrion. Altogether, these results are fully consistent with predictions arising from experiments performed with purified ATP synthase reconstituted into proteoliposomes and lipid bilayers. It is important to point out that this tight consistency of results obtained between the technically diverse range of experiments presented here (i.e., from single molecule to intact organelle approaches) rules out that the behavior of purified, isolated F_1F_0 develops an artifactual K^+ conductance (e.g., due to some hypothetical loss of an important regulatory component, etc.), because ATP synthase undoubtedly remains naturally and functionally unaltered in the intact mitochondrial experiments.

Discussion

Up to the present, it has been a central tenet of bioenergetics that mammalian ATP synthase operates solely on proton flux through F_0 to make ATP. The present work significantly revises that concept. We found that despite the high degree of F_0 's H^+ selectivity vs. K^+ ($\sim 10^6:1$), the abundance of cytoplasmic K^+ over H^+ being $> 10^6:1$ enables ATP synthase to harness $\Delta\mu_K$ (electrical gradient energy) and conduct a significant number of K^+ for every H^+ in the synthesis of ATP. Specifically, our finding is supported by the following evidence: 1) under physiological pH = 7.2 and $K^+ = 140$ mEq/L conditions, purified F_1F_0 reconstituted in proteoliposomes exhibiting a stable (non-zero) $\Delta\Psi_m$ in the presence of the K^+ gradient, can synthesize ATP solely driven by the free energy stored in the experimentally-defined K^+ gradient by up to $\sim 3.5 K^+$ for every H^+ ; 2) purely

K^+ -driven ATP synthesis from single F_1F_0 molecules measured by bioluminescence photon detection could be directly demonstrated along with simultaneous measurements of unitary K^+ currents by voltage clamp, both blocked by specific F_0 inhibitors, Vent/Oligo; 3) in the presence of K^+ , compared to osmotically-matched conditions in which this cation is absent, isolated mitochondria display 3.5 or 3.7-fold higher rates of ATP synthesis, at the expense of 2.6- or 1.7-fold higher rates of oxygen consumption in G/M or PCoA, respectively, these fluxes being driven by a 2.7:1 K^+ : H^+ stoichiometry; the excellent agreement between the functional data obtained from purified F_1F_0 single molecule experiments and ATP synthase studied in the intact mitochondrion under unaltered OxPhos coupling by K^+ presence, is entirely consistent with K^+ transport through the ATP synthase driving the observed increase in ATP synthesis.

Further work from our lab addresses the regulation of K^+ transport flux through the ATP synthase by endogenous regulatory proteins, in addition to pharmacological agents that have been conventionally used to characterize the mitochondrial K_{ATP} channel (Juhaszova et al.¹⁴). Therein, we provide evidence of evolutionary convergence of ATP synthase regulatory proteins with the emergence of mitochondria to suggest a selection process favoring mechanisms that avoid energy wastage and improve the activity and efficiency of the ATP synthase.

As the currency of metabolic energy, the flux of ATP catalyzed by ATP synthase generates every day (in humans) $\sim 1 \times 10^{26}$ ATP molecules, corresponding to a mass of about 80 kg. In other words, each day we synthesize and recycle the equivalent of our own body weight in ATP.⁴⁰ In the human heart, the estimated daily amount of ATP generated (6–35 kg) is much more than its own weight (~ 300 g).^{41,42} This entails an extraordinary process of energy supply-demand matching which occurs at extremely high rates. The increase in energy demand from rest to maximal can be 5- to 10-fold in normal people, depending on the intensity of physical activity, and reach 20-fold in well-trained human athletes.⁴³ We propose that the dynamic range of ATP synthesis flux enabled through the newly discovered K^+ mechanisms described here, are essential to fulfill to a great extent the broad span of energy demand needs, matched by the supply of a highly efficient mechanism of energy generation, and evolutionarily tuned by endogenous regulators from the Bcl2 family of proteins.

Although what we propose remains fully compatible with Mitchell's chemiosmotic mechanism¹²; reviewed in¹³, our findings have major bioenergetic implications (conceptualized in Figure 6). Electrophysiological measurements indicate that purified F_1F_0 reconstituted into the lipid bilayer could conduct up to 3.7 K^+ for every H^+ (see section, Measurement of unitary K^+ and H^+ currents from F_1F_0) in the absence of any other K^+ conducting pathway (see section, Potassium channel openers activate K^+ flux into proteoliposome-reconstituted ATP synthase, Figure S2 and Figure 1C). The demonstration that F_1F_0 in isolated mitochondria utilizes $\sim 3 K^+$ for every H^+ transferred, yielding $\sim 2 K^+$ per ATP (based on 8 ions driving the c-ring per 3 ATPs in mammalian F_1F_0 together with our measurement of $\sim 3:1 K^+$: H^+), indicates that ATP synthase acts as a K^+ -uniporter, i.e., the primary way for K^+ to enter mitochondria. In isolated mitochondria the major fraction of the total K^+ flux (likely significantly exceeding 60% considering the accompanying large differences in matrix volume changes) is sustained by the ATP synthase (Figure 5; Figure S4B and D), thus showing that F_1F_0 is a major

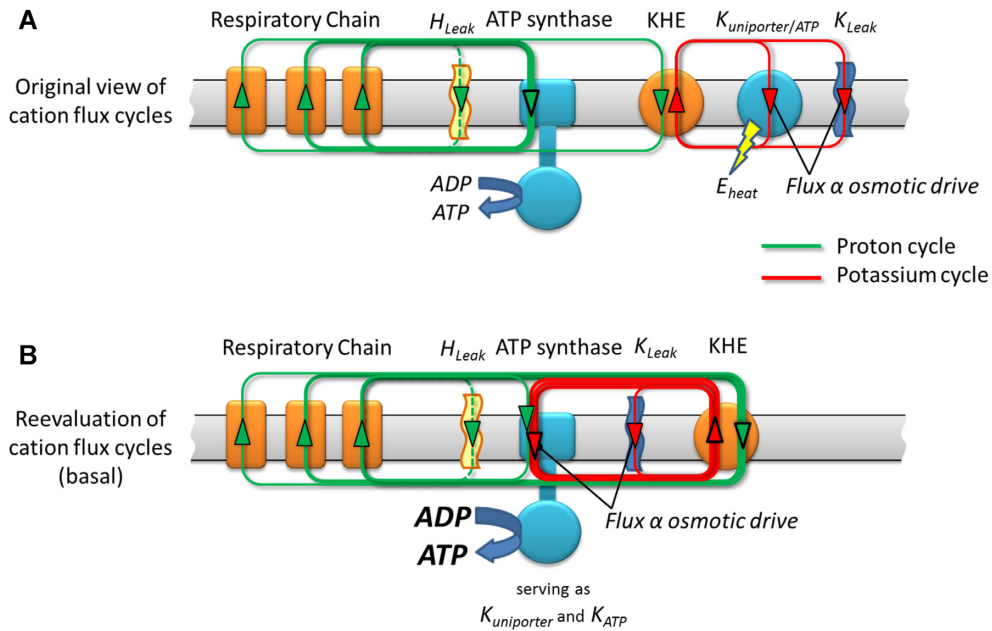


Figure 6. Scheme of the H^+ and K^+ transport across the inner mitochondrial membrane. From the energetic standpoint, all the energy available to perform work and execute the ionic movements derives from the original H^+ gradient established by proton pumps in the respiratory chain. A central point is the obligatory preservation of charge and mass balance under the steady state circuits. In the “original view of cation flux cycles” (A), a certain (majority) of the H^+ gradient is being harnessed by F_1F_0 directly to make ATP, whereas a certain amount of K^+ is entering the matrix through an ordinary K^+ channel mechanism (a “ mK_{ATP} -uniporter” channel), driven by $\Delta\Psi$, and extruded via KHE utilizing the energy remaining in the fraction of the H^+ gradient not harnessed by F_1F_0 . The equivalent energy of this fraction being used to extrude K^+ , and a large fraction of that non-ATP-producing energy would essentially be dissipated as heat in the constant cycle of K^+ recirculation (red circuit in A). In the new mechanism (B) the same amount of energy available in the original H^+ gradient but largely lost as heat is entirely available to produce ATP, simply by having the mK_{ATP} -uniporter mechanism reside inside, and as natural part of, F_1F_0 with the traffic of H^+ or K^+ contributing its energy to producing ATP. The remainder of the H^+ gradient energy is now utilized to remove all the K^+ that entered via F_1F_0 (n.b., this exchange process of extruding K^+ , restoring $\Delta\mu_K$, is the way that the H^+ gradient energy is still the original, entire driving force for ATP production). However, the gain is that more ATP is produced for the same input energy by not wasting some of that energy on maintaining what was originally thought to be a separate K^+ cycle that does not/cannot generate any ATP. Engineered this way, it is a better, tightly coupled system of energy supply-demand matching through the K^+ cycle utilizing F_1F_0 because the matrix influx of K^+ is truly directly proportional to ATP synthesis.

mitochondrial K^+ influx pathway. Since K^+ entry is directly proportional to ATP synthesis and regulates matrix volume and respiration, in turn it directs the matching between energy supply and demand (see further discussion, below). The K^+ flux can be enhanced, halted, or even reversed depending on ATP concentration based on thermodynamic energy balance (and the function of IF_1).

Since mammalian ATP synthase is currently believed to be a machine running exclusively on H^+ , the present work, for the first time, to our knowledge, shows that ATP synthase utilizes $\sim 3 K^+$ for every H^+ to make ATP inside intact cellular mitochondria. This K^+ entry is directly proportional to ATP synthesis ($\sim 2 K^+$ per ATP) and regulates matrix volume, and in turn serves the function of directing the *matching of cellular energy utilization with its production*. In particular, an increase in cellular workload leads to an increase in ATP demand (and ADP accumulation) and an increase in ATP synthase activity which in turn causes a *significant but reversible matrix contraction* (Figure S4 H, I, L, M) which if unopposed by inward K^+ flux probably tends to limit respiration and ATP production (Figure S4 L, M). A sudden increase in ATP synthase activity causes a transient matrix K^+ influx > efflux mismatch (Figure S4 B, D) leading to (osmotically driven) net water retention, which attenuates the degree of matrix contraction (compare matrix volume dynamics in K^+ vs sucrose media, Figure S4 L, M) and supports a better matching of respiratory drive to maintain the increased utilization of the electrochemical gradient energy by ATP synthase (compare

ATP synthesis capacities in K^+ vs sucrose media, Figure 5C). Further work from our laboratory Juhaszova et al.¹⁴ presents additional evidence supporting this mechanism which is the basis of the regulatory process of volume activation of respiration (e.g., as described and characterized in^{44,45}). After a brief time, KHE catches up restoring K^+ influx-efflux matching which nulls the osmotic imbalance and stops additional changes in volume, but remaining at an elevated matrix volume together with a higher level of respiratory function to better support OxPhos demands than if K^+ were absent (Figure 5A and S4 E-G). When workload and ATP consumption return to normal levels, the decrease in ATP synthase activity and its accompanying proportionally reduced rate of K^+ influx causes a transient K^+ influx < efflux mismatch causing a reversal of osmotic forces (now outward) and allowing the matrix volume and respiration to return to the baseline. These mechanisms lead to improved matrix volume compensation and regulated respiratory function matching to ATP synthase activity during high workloads which leads to a ~ 3 -fold increase in ATP output in K^+ vs sucrose media (Figure 5C). This explains how these newly described mechanisms (Figure 6B) differ from the current dogma (Figure 6A) whilst still conforming completely to Mitchell’s chemiosmotic mechanism.¹²

Although the mitochondrial ATP synthase has been discovered almost a century ago⁴⁶ the precise role of volume changes in the regulation of mitochondrial metabolism is still elusive despite having been repeatedly emphasized.⁴⁷⁻⁴⁹ According to

the results of the present work, K^+ -driven ATP synthesis plays a major role in the osmotic regulation of OxPhos. Whether changes in matrix volume act to enhance respiratory function by recruiting respiratory chain supercomplex formation (e.g.,^{50,51}; reviewed by^{52,53}) or by other mechanisms yet to be elaborated (e.g., see discussion of matrix Na^+ below), is a matter for future study.

The ability to reproduce our experimental results by independent laboratories is another important avenue to gain further confidence in some of the conclusions presented here, e.g., that the molecular entity responsible for mK_{ATP} channel activity is ATP synthase. Thus, we sought to provide such independent evidence by examining published papers by other labs reporting the electrophysiological characterization of the conventionally prepared mK_{ATP} . A PubMed literature search revealed eight papers by five independent labs^{20,21,23-27} which provided sufficient measured parameters allowing us to re-analyze and extract the single ion permeability coefficients, P_H and P_K (cf., Eq. 2 and section Measurement of unitary K^+ and H^+ currents from F_1F_0). Querying the “what if” scenario that both K^+ and H^+ permeate the mK_{ATP} , the values ($n = 9$) extracted from these publications for the permeability coefficients of both protons (P_H) and potassium (P_K) provided excellent quantitative agreement with our data, further supporting our conclusions regarding the identity of mK_{ATP} channel.

Regarding the issue of a transporter (e.g., ATP synthase) functioning as an ion channel by its biophysically characterized electrophysiological behavior (based on the activities we have measured and extensively verified as not being caused by a contaminant), this is just the latest example of a growing list of “classical” transporters that have been identified in the past 2 decades as having “dual use” because of their accompanying channel activity⁵⁴; see also⁵⁵). Other well characterized examples of dual-use transporters with channel behavior include, (i) GABA transporters with cation-permeable channels,⁵⁶ (ii) serotonin transporters with Na^+ channel activity,⁵⁷ (iii) norepinephrine transporters with inorganic ion permeable channels,⁵⁸ (iv) dopamine transporters with Cl^- channel activity,⁵⁹ (v) certain members of the ClC chloride channel family which function as H^+/Cl^- exchangers,⁶⁰ (vi) Na/K pump with proton conducting channels,⁶¹ (vii) the cystic fibrosis transmembrane conductance regulator (CFTR) which operates as a Cl^- channel gated by its ATPase activity,⁶² (viii) TMEM16 proteins encompassing both Cl^- channel and lipid scramblase activity,⁶³ (ix) glutamate transporters with Cl^- channel activity,⁶⁴ (x) the organic anion (prostaglandin) transporter SLCO2A1 that is a core component of the Maxi-Cl channel,⁶⁵ and (xi) acetate transporters with Cl^- channel activity.⁶⁶ To this growing and important list, we add mammalian ATP synthase whose activity mimics a monovalent cation channel as described herein (i.e., for H^+ , and at ~ 1 million-fold lower permeability, K^+ (and Na^+)).

A long debated issue in the chemiosmotic hypothesis has been about the proton gradient being localized or delocalized (reviewed by⁶⁷). Recently, the use of a ratiometric pHluorin, a GFP protein pH sensor directed to specific mitochondrial subcompartments, has shown the presence of only very small pH gradients generated in the unstirred layers close to membranes.⁶⁸ These authors suggest that kinetic coupling involving a “lateral membrane proton diffusion” between the $\Delta\mu_H$ generator (respiratory chain) and the ATP synthase, rather than local proton gradients, may be involved in ATP synthesis. However, under the conditions used in our planar membranes or proteoliposomes there are no “generators” of $\Delta\mu_H$. Thus, the

only driving force for ATP synthesis would be the transmembrane gradient of K^+ and/or H^+ bulk phases. The experimental results obtained with intact, functional, mitochondria under steady state conditions are also consistent with single molecule and proteoliposome experiments, and can be interpreted without invoking local H^+ gradients. Ultimately the predictions from single molecule and proteoliposome-reconstituted experiments are in full agreement with the intact mitochondrial results.

Recent high-resolution structures of dimeric ATP synthase from *Polytomella* alga and bovine mitochondria indicate that the matrix and luminal half-channels of the proton conducting pathway are likely hydrated with water molecules all the way to the positively charged Arg¹⁵⁹ (in bovine, and to the corresponding Arg²³⁹ in *Polytomella*) separating these channels. In the reconstruction of the *Polytomella* proton channel, the narrowest part from the luminal half-channel is 4 by 5 Å, and the narrowest part from the matrix half-channel is 4 by 7 Å.⁶⁹⁻⁷¹ In view of these results and considering that “water-naked” K^+ ion has a radius of 1.33 Å (~ 4 Å singly hydrated) and 0.95 Å for Na^+ (3.67 Å singly hydrated), in principle, ion size per se is not a limitation for K^+ (or Na^+) ion to move through luminal and matrix part of the proton conducting channel of the ATP synthase. Thus, by extension of this analysis to mammalian ATP synthase, there would be no theoretical, strict size-prohibition for the single-hydrated K^+ or Na^+ (in addition to the typical H^+) to pass through the mammalian ATP synthase hemichannels, which of course is compatible with the data presented in the present report. The precise basis of the relative ion selectivity ($\sim 10^6$ -fold for hydrated- H^+ over hydrated- K^+ and $-Na^+$) remains to be determined, but as with other selective ion channels, it might involve the relative energy barriers generated by the differences in dehydration energy, and the degree to which the “solvation environment” and geometry of functional side chains on the narrow protein neck of the selectivity filter—where the (likely singly-hydrated-) ions pass single-file—matches each of the respective ions’ preferred coordination chemistry at a distance relevant to favorable (i.e., energy barrier-minimizing) ligand-interactions (the net effect of which overwhelmingly favors H^+ transit). The vast excess of cytoplasmic K^+ and Na^+ over H^+ overcomes these oppositely-biased selectivity factors, and enables the roughly comparable levels of macroscopic ion fluxes observed for each of these species.

To exert its inhibitory action, DCCD modifies the F_0 part of ATP synthase through a protonated glutamate (E58) in the c-ring. The protonated requirement for inhibition is corroborated by the results in Figure 3 in which, under the conditions of exclusive K^+ transport, does not enable DCCD current inhibition in the planar lipid membrane system. A previous report in *P. modestum*²⁸ described that, in the presence of Na^+ or Li^+ , ATP synthase was specifically protected from inhibition by DCCD. E58 is not the only site of ATP synthase modified by DCCD. Glutamate E203 in the β -subunit in F_1 (E199 in⁷²) can also be modified by DCCD, and the effects of such modification are unknown. An increase in the current upon DCCD addition has been observed which, speculatively, may result from the interaction of DCCD with E203 (Figure 3). Our observations are consistent with published information, since an increase in rotation following DCCD addition has been observed elsewhere.⁷³

Another interesting question is the possible role(s) played by the likely utilization of a relatively small quantity of Na^+ (its free energy across the mitochondrial inner membrane essentially determined by $\Delta\Psi_m$, as with K^+) by mammalian F_1F_0 to make ATP at normal cytoplasmic Na^+ levels. We measured P_{Na}

to be approximately the same as P_K (see section Measurement of unitary K^+ and H^+ currents from F_1F_0 , and Figure 2E), so at cytoplasmic Na^+ levels of 8, 10 or 12 mEq/L,^{74,75} we would expect ATP synthase to conduct ~one Na^+ for every 5, 4 or 3 H^+ , respectively, during the synthesis of ATP in normally charged cellular mitochondria (i.e., at $\Delta\Psi_m$ magnitudes > 100 mV). At these possible levels, it might not be a trivial epi-phenomenon, and since the flux of Na^+ , like K^+ , would vary in direct proportion to workload and ATP synthase activity, matrix Na^+ levels could be significantly altered in this way, (i) regulating OxPhos via a recently identified mechanism involving a direct action of matrix Na^+ on lipids to change inner membrane fluidity and respiratory chain function,⁷⁶ and (ii) biasing mitochondrial NCX activities, and in turn, factoring as a previously unrecognized workload-related determinant of matrix Ca^{2+} levels. Since mitochondrial Ca^{2+} is a significant regulator of several Krebs cycle dehydrogenases (reviewed in⁷⁷), both of these potential Na^+ mechanisms could play direct roles in energy homeostasis, and, for example, be important in heart failure where a limitation of energy production is thought to play a significant pathological role and cytoplasmic Na^+ can achieve abnormally elevated levels. This hypothesis could be the subject of future research.

In conclusion, we demonstrated that mitochondrial ATP synthase utilizes the ion gradient energy not only of H^+ but also of K^+ to drive ATP synthesis, what is likely to be the primary mechanism by which mitochondrial function matches energy supply with demand for all cells in the body. The essential mitochondrial homeostatic and pro-survival mechanisms discussed here and in Juhaszova et al.,¹⁴ including F_1F_0 operation as a primary mitochondrial K^+ uniporter to facilitate energy supply-demand matching, and as a recruitable mK_{ATP} channel to protect from pathological opening of the mPTP, result from regulated function of ATP synthase conducting both K^+ and H^+ .

METHODS

Detailed methods are provided in the Supplemental Information Section of this manuscript.

Purification, Characterization and Reconstitution of F_1F_0

F_1F_0 was purified according to manufacturer protocol (MitoSciences) and reconstituted into liposomes and planar lipid membranes. Isolated F_1F_0 was characterized by gel electrophoresis using the Novex Bis-tris gel systems under native and denaturing conditions following the manufacturer protocol (Invitrogen). Mice carrying an inactivated *Atp1f1* allele were obtained from the European Mouse Mutant Archive (EMMA), bred to homozygosity and are referred to as $IF1^{-/-}$ or $IF1$ depleted.

ATP Measurements

Bioluminescent assays which employ the luciferin-luciferase ATP-dependent reaction were used to evaluate the ATP production by PL.

Electrophysiological Measurements

The Planar Lipid Bilayer workstations (Warner Instruments) were used to characterize electrophysiological properties of the reconstituted F_1F_0 .

Simultaneous measurements of unitary K^+ currents and single photon detection of ATP synthesis activity (bioluminescence)

from reconstituted F_1F_0 into a lipid hydrogel-hydrogel interface bilayer formed on a 30-50 μm glass pipette are described in SI Supplemental text.

Membrane Potential Measurements

The potential-sensitive fluorescent probe oxonol VI was used to monitor F_1F_0 -generated $\Delta\psi$ in a K^+ gradient using a PTI spectrofluorometer (Photon Technology International Inc.).

Statistics

All experiments were performed at least in triplicate, with cell number greater than 12 in each independent experiment unless stated otherwise. All data are mean \pm SEM. Comparisons within groups were made by an appropriate one-way ANOVA or Student t test, and P value <0.05 was considered as statistically significant.

Supplementary Material

Supplementary material is available at the *APS Function* online.

Funding

This work was supported entirely by the Intramural Research Program, National Institute on Aging, NIH.

Acknowledgments

We thank E.G. Lakatta for useful discussions, D. Boyer for animal husbandry, L. Rezanka for mice genotyping and M.J. del Hierro Sanchez for assistance in obtaining the transgenic $IF1^{-/-}$ mice.

Author Contributions

Conceptualization, M.J., D.B.Z. and S.J.S.; Methodology, M.J., E.K., H.B.N., K.W.F., L.M., M.A.A., S.C. and S.J.S.; Software, Y.Y., S.B.G. and S.C.; Formal Analysis, Y.Y., S.B.G., S.C. and S.J.S.; Investigation, M.J., E.K., D.B.Z., H.B.N., M.A.A. and S.C.; Resources, R.d.C., L.M., S.B.G. and S.J.S.; Writing-Original Draft, S.J.S.; Writing-Review & Editing, M.J., E.K., D.B.Z., K.W.F., R.d.C., S.B.G., M.A.A., S.C. and S.J.S.; Visualization, M.J., E.K., Y.Y., S.B.G., M.A.A., S.C. and S.J.S.; Supervision, S.J.S.

Competing Interest Statement

The authors declare that they have no conflict of interest.

Data Availability

The underlying data of this article are available in the article, and its online Supplementary Material. Any other data request will be shared by the corresponding author, Dr. Sollott, SJ, upon reasonable request.

References

1. Cross RL, Muller V. The evolution of A-, F-, and V-type ATP synthases and ATPases: reversals in function and changes in the H^+ /ATP coupling ratio. *FEBS Lett* 2004;576(1-2):1-4. http://www.ncbi.nlm.nih.gov/entrez/query.fcgi?cmd=Retrieve&db=PubMed&dopt=Citation&list_uids=15473999.

2. Stock D, Leslie AG, Walker JE. Molecular architecture of the rotary motor in ATP synthase. *Science* 1999;286(5445):1700–1705. http://www.ncbi.nlm.nih.gov/entrez/query.fcgi?cmd=Retrieve&db=PubMed&dopt=Citation&list_uids=10576729.
3. Kuhlbrandt W, Davies KM. Rotary ATPases: a New Twist to an Ancient Machine. *Trends Biochem Sci* 2016;41(1):106–116.
4. Boyer PD. The ATP synthase—a splendid molecular machine. *Annu Rev Biochem* 1997;66(1):717–749. http://www.ncbi.nlm.nih.gov/entrez/query.fcgi?cmd=Retrieve&db=PubMed&dopt=Citation&list_uids=9242922.
5. Abrahams JP, Leslie AG, Lutter R, Walker JE. Structure at 2.8 Å resolution of F1-ATPase from bovine heart mitochondria. *Nature* 1994;370(6491):621–628.
6. Noji H, Yasuda R, Yoshida M, Kinoshita K, Jr. Direct observation of the rotation of F1-ATPase. *Nature* 1997;386(6622):299–302. http://www.ncbi.nlm.nih.gov/entrez/query.fcgi?cmd=Retrieve&db=PubMed&dopt=Citation&list_uids=9069291.
7. Kaim G, Dimroth P. A double mutation in subunit c of the Na(+)-specific F1F0-ATPase of *Propionigenium modestum* results in a switch from Na+ to H(+)-coupled ATP synthesis in the *Escherichia coli* host cells. *J Mol Biol* 1995;253(5):726–738. http://www.ncbi.nlm.nih.gov/entrez/query.fcgi?cmd=Retrieve&db=PubMed&dopt=Citation&list_uids=7473747.
8. Leone V, Pogoryelov D, Meier T, Faraldo-Gomez JD. On the principle of ion selectivity in Na+/H+-coupled membrane proteins: experimental and theoretical studies of an ATP synthase rotor. *Proc Natl Acad Sci U S A* 2015;112(10):E1057–1066.
9. Feniouk BA, Kozlova MA, Knorre DA, Cherepanov DA, Mulikjanian AY, Junge W. The proton-driven rotor of ATP synthase: ohmic conductance (10 fS), and absence of voltage gating. *Biophys J* 2004;86(6):4094–4109. http://www.ncbi.nlm.nih.gov/entrez/query.fcgi?cmd=Retrieve&db=PubMed&dopt=Citation&list_uids=15189903.
10. Hille B. *Ion Channels of Excitable Membranes*. 3rd ed: Sinauer Associates, Inc.; Sunderland, MA 01375, USA 2001.
11. Garlid KD, Dos Santos P, Xie ZJ, Costa AD, Pauczek P. Mitochondrial potassium transport: the role of the mitochondrial ATP-sensitive K(+) channel in cardiac function and cardioprotection. *Biochim Biophys Acta* 2003;1606(1-3):1–21. <http://www.ncbi.nlm.nih.gov/pubmed/14507424>.
12. Mitchell P. Coupling of phosphorylation to electron and hydrogen transfer by a chemi-osmotic type of mechanism. *Nature* 1961;191(4784):144–148. <http://www.ncbi.nlm.nih.gov/pubmed/13771349>.
13. Nicholls DG, Ferguson SJ. *Bioenergetics (Fourth Edition)*. Academic Press; 32 Jamestown Road, London NW1 7BY, UK. 2013.
14. Juhaszova M, Kobrinsky E, Zorov DB, et al. ATP synthase K+- and H+-fluxes drive ATP synthesis and enable mitochondrial K+-“uniporter” function: II. Ion and ATP synthase flux regulation. *Function (Oxf)* 2022. doi: <https://doi.org/10.1093/function/zqac001>.
15. Foster DB, Ho AS, Rucker J, et al. Mitochondrial ROMK channel is a molecular component of mitoK(ATP). *Circ Res* 2012;111(4):446–454.
16. Jiang MT, Ljubkovic M, Nakae Y, et al. Characterization of human cardiac mitochondrial ATP-sensitive potassium channel and its regulation by phorbol ester in vitro. *Am J Physiol Heart Circ Physiol* 2006;290(5):H1770–H1776. PM:16361367.
17. Nakae Y, Kwok WM, Bosnjak ZJ, Jiang MT. Isoflurane activates rat mitochondrial ATP-sensitive K+ channels reconstituted in lipid bilayers. *Am J Physiol Heart Circ Physiol* 2003;284(5):H1865–H1871. PM:12573994.
18. Grigoriev SM, Skarga YY, Mironova GD, Marinov BS. Regulation of mitochondrial KATP channel by redox agents. *Biochim Biophys Acta* 1999;1410(1):91–96. PM:10076019.
19. Mironova GD, Skarga YY, Grigoriev SM, Negoda AE, Kolomytkin OV, Marinov BS. Reconstitution of the mitochondrial ATP-dependent potassium channel into bilayer lipid membrane. *J Bioenerg Biomembr* 1999;31(2):159–163. http://www.ncbi.nlm.nih.gov/entrez/query.fcgi?cmd=Retrieve&db=PubMed&dopt=Citation&list_uids=10449243.
20. Ardehali H, Chen Z, Ko Y, Mejia-Alvarez R, Marban E. Multi-protein complex containing succinate dehydrogenase confers mitochondrial ATP-sensitive K+ channel activity. *Proc Natl Acad Sci USA* 2004;101(32):11880–11885.
21. Bednarczyk P, Dolowy K, Szewczyk A. Matrix Mg2+ regulates mitochondrial ATP-dependent potassium channel from heart. *FEBS Lett* 2005;579(7):1625–1632. PM:15757652.
22. Bednarczyk P, Kicinska A, Kominkova V, Ondrias K, Dolowy K, Szewczyk A. Quinine inhibits mitochondrial ATP-regulated potassium channel from bovine heart. *J Membr Biol* 2004;199(2):63–72.
23. Inoue I, Nagase H, Kishi K, Higuti T. ATP-sensitive K+ channel in the mitochondrial inner membrane. *Nature* 1991;352(6332):244–247.
24. Kicinska A, Swida A, Bednarczyk P, et al. ATP-sensitive potassium channel in mitochondria of the eukaryotic microorganism *Acanthamoeba castellanii*. *J Biol Chem* 2007;282(24):17433–17441.
25. Kulawiak B, Bednarczyk P. Reconstitution of brain mitochondria inner membrane into planar lipid bilayer. *Acta Neurobiol Exp (Wars)* 2005;65(3):271–276. <http://www.ncbi.nlm.nih.gov/pubmed/16130801>.
26. Miedema H, van Walraven HS, de Boer AH. Potassium selective and venturicidin sensitive conductances of Fo purified from bovine heart mitochondria, reconstituted in planar lipid bilayers. *Biochem Biophys Res Commun* 1994;203(2):1005–1012. <http://www.ncbi.nlm.nih.gov/pubmed/8093018>.
27. Zhang DX, Chen YF, Campbell WB, Zou AP, Gross GJ, Li PL. Characteristics and superoxide-induced activation of reconstituted myocardial mitochondrial ATP-sensitive potassium channels. *Circ Res* 2001;89(12):1177–1183. <http://www.ncbi.nlm.nih.gov/pubmed/11739283>.
28. Kluge C, Dimroth P. Specific protection by Na+ or Li+ of the F1F0-ATPase of *Propionigenium modestum* from the reaction with dicyclohexylcarbodiimide. *J Biol Chem* 1993;268(20):14557–14560. http://www.ncbi.nlm.nih.gov/entrez/query.fcgi?cmd=Retrieve&db=PubMed&dopt=Citation&list_uids=8392053
29. Pogoryelov D, Krah A, Langer JD, Yildiz O, Faraldo-Gomez JD, Meier T. Microscopic rotary mechanism of ion translocation in the F(o) complex of ATP synthases. *Nat Chem Biol* 2010;6(12):891–899.
30. Symersky J, Pagadala V, Osowski D, et al. Structure of the c(10) ring of the yeast mitochondrial ATP synthase in the open conformation. *Nat Struct Mol Biol* 2012;19(5):485–491, S481.
31. Davies KM, Strauss M, Daum B, et al. Macromolecular organization of ATP synthase and complex I in whole mitochondria. *Proc Natl Acad Sci USA* 2011;108(34):14121–14126.

32. Couoh-Cardel SJ, Uribe-Carvajal S, Wilkens S, Garcia-Trejo JJ. Structure of dimeric F1F0-ATP synthase. *J Biol Chem* 2010;**285**(47):36447–36455.
33. Watt IN, Montgomery MG, Runswick MJ, Leslie AG, Walker JE. Bioenergetic cost of making an adenosine triphosphate molecule in animal mitochondria. *Proc Natl Acad Sci* 2010;**107**(39):16823–16827. http://www.ncbi.nlm.nih.gov/entrez/query.fcgi?cmd=Retrieve&db=PubMed&dopt=Citation&list_uids=20847295.
34. Diez M, Zimmermann B, Borsch M, et al. Proton-powered subunit rotation in single membrane-bound F0F1-ATP synthase. *Nat Struct Mol Biol* 2004;**11**(2):135–141.
35. Etzold C, Deckers-Hebestreit G, Altendorf K. Turnover number of *Escherichia coli* F0F1 ATP synthase for ATP synthesis in membrane vesicles. *Eur J Biochem* 1997;**243**(1-2):336–343. <https://www.ncbi.nlm.nih.gov/pubmed/9030757>.
36. Junesch U, Graber P. The rate of ATP-synthesis as a function of delta pH and delta psi catalyzed by the active, reduced H(+)-ATPase from chloroplasts. *FEBS Lett* 1991;**294**(3):275–278. <https://www.ncbi.nlm.nih.gov/pubmed/1661688>.
37. Soga N, Kinoshita K, Jr., Yoshida M, Suzuki T. Kinetic equivalence of transmembrane pH and electrical potential differences in ATP synthesis. *J Biol Chem* 2012;**287**(12):9633–9639.
38. Cortassa S, Aon MA, Marban E, Winslow RL, O'Rourke B. An integrated model of cardiac mitochondrial energy metabolism and calcium dynamics. *Biophys J* 2003;**84**(4):2734–2755. http://www.ncbi.nlm.nih.gov/entrez/query.fcgi?cmd=Retrieve&db=PubMed&dopt=Citation&list_uids=12668482
39. Wei AC, Aon MA, O'Rourke B, Winslow RL, Cortassa S. Mitochondrial energetics, pH regulation, and ion dynamics: a computational-experimental approach. *Biophys J* 2011;**100**(12):2894–2903.
40. Rich P. Chemiosmotic coupling: the cost of living. *Nature* 2003;**421**(6923):583.
41. Ashrafian H, Frenneaux MP, Opie LH. Metabolic mechanisms in heart failure. *Circulation* 2007;**116**(4):434–448.
42. Taegtmeyer H. Energy metabolism of the heart: from basic concepts to clinical applications. *Curr Probl Cardiol* 1994;**19**(2):61–86. <https://www.ncbi.nlm.nih.gov/pubmed/8174388>.
43. Weibel ER, Hoppeler H. Exercise-induced maximal metabolic rate scales with muscle aerobic capacity. *J Exp Biol* 2005;**208**(Pt 9):1635–1644.
44. Garlid KD, Paucek P. Mitochondrial potassium transport: the K(+) cycle. *Biochim Biophys Acta* 2003;**1606**(1-3):23–41. <http://www.ncbi.nlm.nih.gov/pubmed/14507425>.
45. Juhaszova M, Zorov DB, Kim SH, et al. Glycogen synthase kinase-3beta mediates convergence of protection signaling to inhibit the mitochondrial permeability transition pore. *J Clin Invest* 2004;**113**(11):1535–1549. http://www.ncbi.nlm.nih.gov/entrez/query.fcgi?cmd=Retrieve&db=PubMed&dopt=Citation&list_uids=15173880
46. Engelhardt WA. Ortho and pyrophosphate in aerobic and anaerobic metabolism of blood cells. *Biochem Z* 1930;**227**:16–38. <Go to ISI>://WOS:000200826700003.
47. Afzal N, Lederer WJ, Jafri MS, Mannella CA. Effect of crista morphology on mitochondrial ATP output: a computational study. *Current Research in Physiology* 2021;**4**:163–176.
48. Halestrap AP. The regulation of the matrix volume of mammalian mitochondria in vivo and in vitro and its role in the control of mitochondrial metabolism. *Biochim Biophys Acta* 1989;**973**(3):355–382. http://www.ncbi.nlm.nih.gov/entrez/query.fcgi?cmd=Retrieve&db=PubMed&dopt=Citation&list_uids=2647140
49. Srere PA. The Structure of the Mitochondrial Inner Membrane Matrix Compartment. *Trends Biochem Sci* 1982;**7**(10):375–378.
50. Greggio C, Jha P, Kulkarni SS, et al. Enhanced Respiratory Chain Supercomplex Formation in Response to Exercise in Human Skeletal Muscle. *Cell Metab* 2017;**25**(2):301–311.
51. Lapuente-Brun E, Moreno-Loshuertos R, Acin-Perez R, et al. Supercomplex assembly determines electron flux in the mitochondrial electron transport chain. *Science* 2013;**340**(6140):1567–1570.
52. Milenkovic D, Blaza JN, Larsson NG, Hirst J. The Enigma of the Respiratory Chain Supercomplex. *Cell Metab* 2017;**25**(4):765–776.
53. Pfanner N, Warscheid B, Wiedemann N. Mitochondrial proteins: from biogenesis to functional networks. *Nat Rev Mol Cell Biol* 2019;**20**(5):267–284.
54. Minor DL, Jr. Channel surfing uncovers a dual-use transporter. *EMBO J* 2017;**36**(22):3272–3273.
55. DeFelice LJ, Goswami T. Transporters as channels. *Annu Rev Physiol* 2007;**69**(1):87–112.
56. Cammack JN, Schwartz EA. Channel behavior in a gamma-aminobutyrate transporter. *Proc Natl Acad Sci USA* 1996;**93**(2):723–727.
57. Lin F, Lester HA, Mager S. Single-channel currents produced by the serotonin transporter and analysis of a mutation affecting ion permeation. *Biophys J* 1996;**71**(6):3126–3135.
58. Galli A, Blakely RD, DeFelice LJ. Norepinephrine transporters have channel modes of conduction. *Proc Natl Acad Sci USA* 1996;**93**(16):8671–8676.
59. Carvelli L, McDonald PW, Blakely RD, DeFelice LJ. Dopamine transporters depolarize neurons by a channel mechanism. *Proc Natl Acad Sci USA* 2004;**101**(45):16046–16051.
60. Accardi A, Miller C. Secondary active transport mediated by a prokaryotic homologue of ClC Cl- channels. *Nature* 2004;**427**(6977):803–807.
61. Vedovato N, Gadsby DC. Route, mechanism, and implications of proton import during Na+/K+ exchange by native Na+/K+-ATPase pumps. *J Gen Physiol* 2014;**143**(4):449–464.
62. Liu F, Zhang Z, Csanady L, Gadsby DC, Chen J. Molecular Structure of the Human CFTR Ion Channel. *Cell* 2017;**169**(1):85–95 e88.
63. Picollo A, Malvezzi M, Accardi A. TMEM16 proteins: unknown structure and confusing functions. *J Mol Biol* 2015;**427**(1):94–105.
64. Cater RJ, Ryan RM, Vandenberg RJ. The Split Personality of Glutamate Transporters: a Chloride Channel and a Transporter. *Neurochem Res* 2016;**41**(3):593–599.
65. Sabirov RZ, Merzlyak PG, Okada T, et al. The organic anion transporter SLC02A1 constitutes the core component of the Maxi-Cl channel. *EMBO J* 2017;**36**(22):3309–3324.
66. Sun P, Li J, Zhang X, et al. Crystal structure of the bacterial acetate transporter SatP reveals that it forms a hexameric channel. *J Biol Chem* 2018;**293**(50):19492–19500.
67. Mulkidjanian AY, Heberle J, Cherepanov DA. Protons @ interfaces: implications for biological energy conversion. *Biochim Biophys Acta* 2006;**1757**(8):913–930.
68. Toth A, Meyrat A, Stoldt S, et al. Kinetic coupling of the respiratory chain with ATP synthase, but not proton gradients, drives ATP production in cristae membranes. *Proc Natl Acad Sci U S A* 2020;**117**(5):2412–2421.

69. Klusch N, Murphy BJ, Mills DJ, Yildiz O, Kuhlbrandt W. Structural basis of proton translocation and force generation in mitochondrial ATP synthase. *Elife* 2017;**6**. doi: 10.7554/eLife.33274.
70. Murphy BJ, Klusch N, Langer J, Mills DJ, Yildiz O, Kuhlbrandt W. Rotary substates of mitochondrial ATP synthase reveal the basis of flexible F1-Fo coupling. *Science* 2019;**364**(6446). doi: 10.1126/science.aaw9128.
71. Spikes TE, Montgomery MG, Walker JE. Structure of the dimeric ATP synthase from bovine mitochondria. *Proc Natl Acad Sci USA* 2020;**117**(38): 23519–23526.
72. Gibbons C, Montgomery MG, Leslie AG, Walker JE. The structure of the central stalk in bovine F(1)-ATPase at 2.4 Å resolution. *Nat Struct Biol* 2000;**7**(11): 1055–1061.
73. Toei M, Noji H. Single-molecule analysis of FOF1-ATP synthase inhibited by N,N-dicyclohexylcarbodiimide. *J Biol Chem* 2013;**288**(36):25717–25726.
74. Bers DM, Barry WH, Despa S. Intracellular Na⁺ regulation in cardiac myocytes. *Cardiovasc Res* 2003;**57**(4):897–912.
75. Liu T, Takimoto E, Dimaano VL, et al. Inhibiting mitochondrial Na⁺/Ca²⁺ exchange prevents sudden death in a Guinea pig model of heart failure. *Circ Res* 2014;**115**(1):44–54.
76. Hernansanz-Agustín P, Ramos E, Villa-Piña T, et al. Mitochondrial Na⁺ import controls oxidative phosphorylation and hypoxic redox signalling. *bioRxiv* 2018:385690. doi: 10.1101/385690.
77. Mammucari C, Raffaello A, Vecellio Reane D, Gherardi G, De Mario A, Rizzuto R. Mitochondrial calcium uptake in organ physiology: from molecular mechanism to animal models. *Pflugers Arch* 2018;**470**(8):1165–1179.